PREPARATION AND CHARACTERIZATION OF VANADIUM OXIDES ON CARBON FIBER PAPER AS ELECTRODES FOR PSEUDOCAPACITORS

A Thesis
Presented to
The Academic Faculty

By

Cynthia Eckles Cromer

In Partial Fulfillment
Of the Requirements for the Degree
Master of Science in Materials Science & Engineering

Georgia Institute of Technology

May, 2013

PREPARATION AND CHARACTERIZATION OF VANADIUM OXIDES ON CARBON FIBER PAPER AS ELECTRODES FOR PSEUDOCAPACITORS

Approved by:

Dr. Meilin Liu
School of Materials Science and Engineering
Georgia Institute of Technology

Dr. Faisal Alamgir
School of Materials Science and Engineering
Georgia Institute of Technology

Dr. Preet Singh
School of Materials Science and Engineering
Georgia Institute of Technology

Date Approved: March 20, 2013

ACKNOWLEDGEMENTS

Much appreciation and gratitude to:

Dr. Meilin Liu for guidance, support, wisdom

Gordon Waller, Xiaxi Li, Dr. Jung-Pil Lee and Yolande Berta for assistance with SEM

Ben Rainwater, Gordon Waller, Dr. Mingfei Liu, Dr. Yangping Li and Masood Ebrahimi for assistance with XRD

Dr. Kevin Blinn for assistance with Raman

Dr. Lei Yang for teaching me hydrothermal and solution methods, in memoriam

Dr. Min-Kym Song and Dr. Shuang Chen for experimental methods

The OIT department, for keeping my laptop running

My family, for patience and loving support

The infinite Source, the designer of everything beautiful and remarkable observed during this process

Dr. Faisal Alamgir and Dr. Preet Singh for serving on my thesis committee

** the final step on a long path **

TABLE OF CONTENTS

LIST OF TABLES

LIST OF FIGURES

LIST OF SYMBOLS AND ABBREVIATIONS

A	Amps
C	Capacitance (Farads)
°C	Degrees Celcius
CFP	Carbon Fiber Paper
cm	Centimeter
CNT	Carbon nanotubes
Conc.	Concentration / Concentrated
ConcA	Name given to samples of high concentration and most-acid, lowest pH
ConcN	Name given to samples of high concentration and slightly neutralized, higher pH
CV	Cyclic Voltammetry
dk	Dark
DTA	Differential Temperature Analysis
EDLC	Electrochemical Double Layer Capacitor/Capacitance
F	Farads, unit of capacitance
g	Grams
h or hr	Hour
I	Current (Amps)
IR	Internal Resistance; refers to voltage losses in the electrochemical cell
I-V	Current-Voltage; short name for Galvanic Cycle measurements
IW	Incipient Wetness impregnation method, and round of study based upon it
JCPDS	Joint Committee on Powder Diffraction Standards; along with International Centre of Diffraction Data, the source of X-ray diffraction reference patterns
M	Moles/L, molarity, concentration of solution

min	Minute
Ox.	Oxidation
Q	Charge (coulombs)
redox	Reduction/oxidation
s	Second
S.C. or SC	Specific Capacitance
SEM	Scanning Electron Microscopy
TG	Thermogravimetric analysis
V	Volts
VO_x	Vanadium oxide, generic term when stoichiometry is uncertain or not needed
V(V)	Vanadium in oxidation state 5+; similarly, V(IV), V(III), V(II) representing oxidation states 4+, 3+, and 2+
wt%	Weight %
XRD	X-Ray Diffraction
1:2	The ratio of moles of vanadium to moles of acid equal to 1:2

SUMMARY

Supercapacitors are important electrochemical energy storage devices for microelectronic and telecommunication systems, electric cars, and smart grids. However, the energy densities of existing supercapacitors are still inadequate for many applications. The objective of this study was to study the effect of processing conditions on specific capacitance of supercapacitors based on vanadium oxides coated on carbon fiber papers.

This study was conducted to form easily-fabricated compounds of vanadium oxides which could offer promise as pseudocapacitor material; to nucleate these compounds directly onto inexpensive carbon fiber without binder, using cost-effective processes and minimizing environmental impact. The incipient wetness impregnation technique was used to fabricate the electrodes. Electrochemical performance of the resulting electrodes was tested in a Swagelok-type electrochemical two-electrode cell, and the electrodes were characterized by XRD and SEM. Interesting nanofeatures were formed and the vanadium oxides exhibited pseudocapacitance at a respectable level.

Solutions were mixed under mild heat, deposited onto carbon fiber paper to incipient wetness, and annealed at moderate temperatures. High-concentration solutions formed, upon annealing, nanobelts under acidic conditions, and porous xerogel under partly neutralized conditions. A 1:2 ratio of ammonium vanadate to oxalic acid resulted in nanobelts, and the same mix adjusted with ammonium hydroxide resulted in porous xerogel. The CFP was loaded to approximately 45 wt% as air-dried; after annealing to 250°C for three hours, the loading was reduced to approximately 21 wt% and nanofeatures formed with pseudocapacitance response in electrochemical testing.

Capacitance rose with increased concentration, and was higher for annealed samples than un-annealed samples. The highest specific capacitances attained were approximately 450 F per gram of active material, or 1.0-1.2 F/cm^2, approximately twice as high as prepared bare carbon fiber paper.

CHAPTER 1: INTRODUCTION

1.1. Motivation

Energy storage and management is increasingly important with our ever-growing use of battery-powered devices. This study represents progress towards providing power storage and delivery solutions which are more cost-effective while providing good performance. A necessary function in an energy management system is to provide energy for load spikes and to store energy from demand dips. An emerging energy management system is energy harvesting, in which small amounts of energy are stored and accumulated from the ambient environment. In the case of either energy management or energy harvesting, sometimes energy needs to be stored or released more quickly than batteries can manage.

The focus of this thesis is on pseudocapacitors, an important element of energy management and storage systems. As the name might suggest, pseudocapacitor behavior is in between that of batteries and capacitors. Pseudocapacitors are used to quickly store and release energy.

The materials used in mature technology for pseudocapacitors are ruthenium and carbon. The motivation for focusing on vanadium in this study is chiefly that ruthenium is rare and expensive while vanadium is abundant and inexpensive, and that vanadium oxides can exceed the performance of carbon.

1.2. Research Objectives

The focus of this thesis study was on pseudocapacitors made from vanadium oxide coated on carbon fiber paper. The methods used in this study were binder-free, so there was no barrier between the active material and the charge carrier, and no inactive mass. The focus of this work was to discern the fabrication processes capable of coating the carbon fibers conformally and uniformly with a phase of vanadium oxide which gives optimal electrochemical performance.

The goals were:

1. Coat carbon fiber paper (CFP) with vanadium oxide to make electrodes.
2. Use processes which were cost-effective and of minimal environmental impact.
3. Evaluate the electrochemical performance of the fabricated electrodes.
4. Characterize the microstructure, composition and morphology under various processing conditions.
5. Optimize the fabrication to produce the phase and morphology of vanadium oxide resulting in the best performance.

Unique to this study was the use of concentrated solutions and the incipient wetness method to fabricate electrodes. The phase behavior of vanadium oxide in solution is less documented at high concentrations. Vanadium oxides on CFP are also scarcely documented. Incipient wetness is used more often for catalyst fabrication than for electrode fabrication. It is intended that this thesis add to the body of knowledge contributing to better energy storage devices in the future.

1.3. Organization of the Thesis

Chapter 2- Background provides some background to provide a frame of reference for the study and put forth relevant information from the literature at large. Experimental methods are described in Chapter 3- Methods, and data are summarized in Chapter 4- Results. In Chapter 5- Discussion, trends and correlations are drawn from the study's results. Lastly, Chapter 6- Conclusions summarizes the results of the study and suggests follow-up work.

CHAPTER 2: BACKGROUND

2.1. The energy environment and the role of supercapacitors

This section briefly describes the continuum between batteries and capacitors in order to describe the role of pseudocapacitors. The term "supercapacitors" will be used until "pseudocapacitors" are clarified in the following sections.

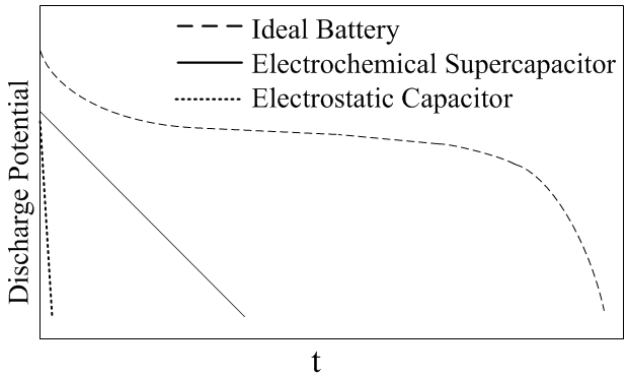

Figure 1. Constant current discharge profile of battery, supercapacitor and capacitor.

Figure 1 shows the characteristic discharge behavior of ideal batteries, supercapacitors and capacitors under constant current. Voltage from an ideal battery is nearly constant over the course of its discharge, but voltage from a capacitor (whether electrostatic or electrochemical) reduces along with the amount of remaining stored charge. [1] The energy storage mechanisms differ as described in Table 1, Figure 3 and the Section 2.1.1.

The role of supercapacitors is to emit or store short bursts of power, with power and speed in between that of batteries and capacitors. Figure 2 indicates how supercapacitors can assist in handling uneven power loads.

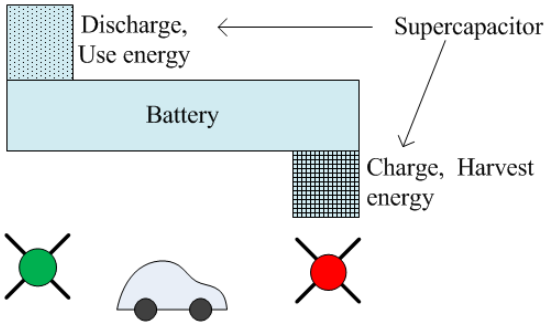

Figure 2. Supercapacitor functions (shaded areas) in an energy profile with peak demands and storage opportunities; example of an electric car in traffic.

Comparing batteries and supercapacitors, batteries store more energy but charge and discharge relatively slowly, while supercapacitors store less energy but charge and discharge much more quickly.

Table 1 lists some common comparisons between batteries, capacitors and supercapacitors. [1] Figure 3 briefly summarizes the differences in charge storage mechanisms.

Table 1. Comparison: energy characteristics of batteries, capacitors and supercapacitors.

	Battery	Standard Capacitor	Super-Capacitor	
Discharge time	0.3-3 h	10^{-3} to 10^{-6} s	0.3-30s	
Charge time	1-5 h	10^{-3} to 10^{-6} s	0.3-30s	
Energy density	10-100	< 0.1	1-10	(Wh/kg)
Specific power	50-200	> 10,000	≈1000	(W/kg)
Cycle life	500-2000	> 500,000	> 100,000	

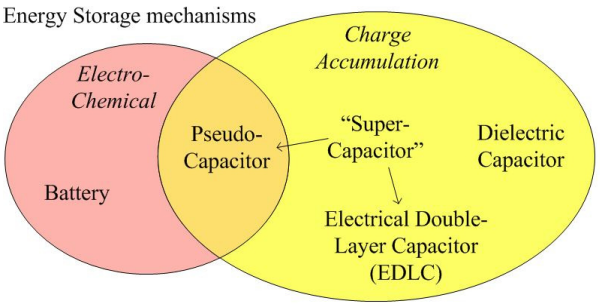

Figure 3. Type of energy storage related to type of storage device.

2.1.1. Batteries. Capacitors and Supercapacitors

Batteries store charge electrochemically. Figure 4 illustrates the intercalation process. Battery power, or potential to deliver energy, is measured in terms of capacity, with units mAh/g.

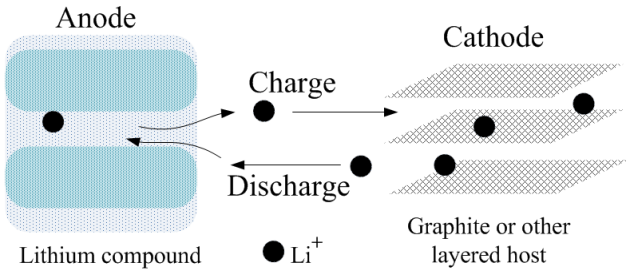

Figure 4. Typical battery storage mechanism: intercalation. After [2].

Capacitors are used to store and deliver charge very quickly, and this potential is measured in terms of capacitance, in units of Farads (Farad = Amp·sec).

In a standard dielectric capacitor, capacitance is created when an electric field creates a charge separation between two metal plates; i.e. charge is accumulated with no movement or chemical changes. Capacitance is a function of the dielectric material, plate area and how small the separation distance can be made. Normal capacitance for standard capacitors is usually on the order of pF (10^{-12}F).

In Electrochemical Double-layer Capacitors (EDLC), charge is accumulated at the electrode surface; the charge separation is no longer across a dielectric, but rather across the nm-thin "double layer" that forms as ions adsorb to the electrode from the electrolyte solution. A separator permits the passage of ions but not electrons. Each electrode develops its own capacitance, and overall the EDLC acts as two capacitors in series.

EDLC capacitors typically have a capacitance of 50μF, over 10^5 times higher than standard electrolytic capacitors. These differences are illustrated in Figure 5.

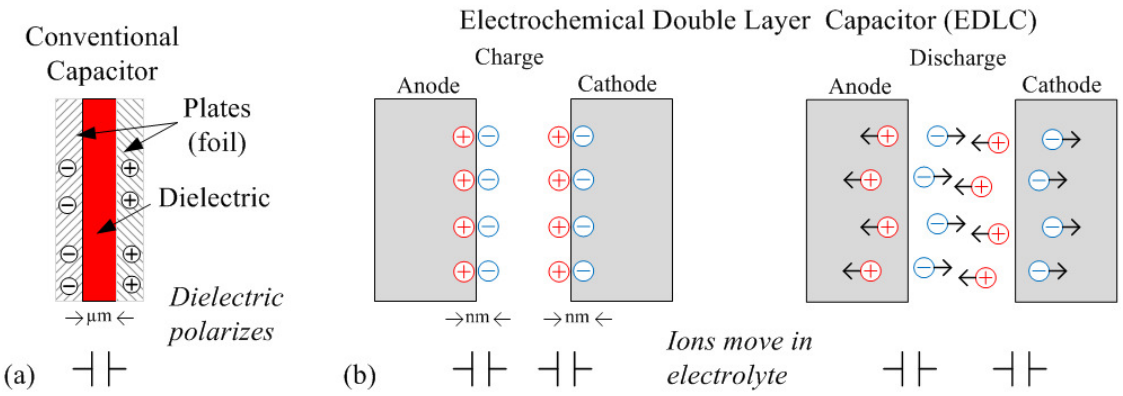

Figure 5. (a) Standard capacitor; (b) Electrochemical Double-Layer Capacitor (EDLC), shown charged and discharging. Blue, negative charge, Red, positive charge.

Pseudocapacitors engage in charge transfer across the electrode-electrolyte interface as described in the next section. "Supercapacitor" is a term loosely used sometimes for pseudocapacitors and sometimes for EDLC capacitors, always differentiating from standard capacitors of pF-strength or below.

2.1.2. Mechanisms of pseudocapacitance

The most written-about mechanism is the most similar to battery action, e.g. intercalation, illustrated in Figure 4. The difference is that in pseudocapacitors, only the top few nm of electrode is involved, not the bulk. Since the bulk is not volumetrically stressed, when surface nanofeatures can accommodate the intercalating ions without distortion, cycling life is much longer than in batteries. To express intercalation in equation form, [3]

$$(V_2O_5)_{surface} + 2M^+ + 2e^- \leftrightarrow (V_2O_5^{2-}\ M_2^{2+})_{surface} \qquad (1)$$

Or, in terms of a commonly studied application of vanadium oxides:

$$Li_xV_2O_5 \leftrightarrow V_2O_5 + xLi + xe^- \quad (2)$$

The principal mechanism of pseudocapacitance is charge transfer across the surface-electrolyte interface. This often happens via reduction-oxidation reactions between the electrode surface and the electrolyte. A typical reduction reaction involving V_2O_5 and an acid would be:

$$\underset{\text{Valence}\quad 5+}{V_2O_5} + 4H^+ \rightarrow \underset{4+}{2VO_2^+} + 2H_2O \quad (3)$$

In this reaction, acid reduces V(V) to V(IV).

A possible faradaic reaction in aqueous electrolyte could be (after [4]):

$$V_2O_5\text{-}0.5H_2O + xM^+ + xe^- \leftrightarrow M_xV_2O_5\text{-}0.5H_2O \quad (4)$$

Other mechanisms of pseudocapacitance are adsorption and chemisorption. Adsorption is highly reversible, a two-dimensional mechanism in which atoms from solution reside against the electrode surface, but they do not become a part of the surface. The voltage response is coverage-dependent, and the resulting capacitance is 10-100 times greater than EDLC. The capacitance can be represented as:

$$C_\theta = Q(d\theta/dV) \quad (5)$$

Where coverage is denoted by θ, with values 0-1 (1 is a monolayer), and Q represents the charge required (Faradaic, crossing between surface and electrolyte) to adsorb or desorb a layer, e.g. of H. Adsorption is different from EDLC because charge is transferred. An example of a surface adsorption event would be: [5]

$$\underset{\text{free surface}}{Pt} + \underset{\text{potential}}{H_3O^+} + e^- \leftrightarrow \underset{\text{occupied surface}}{PtH_{ads}} + H_2O \quad (6)$$

Chemisorption is similar to adsorption in that it is an interaction with surface sites; but orbitals overlap, the bond is short-range and strong, and it takes (and stores)

more energy and time to incorporate ions into the surface layer. Capacitance via chemisorption has the same coverage dependence as adsorption. [5]

2.2. Vanadium

Among materials for pseudocapacitor electrodes, the highest performance is delivered by ruthenium oxides. Ruthenium is a transition metal with high conductivity. Its oxides have been shown to exhibit high specific capacitance over a long cycle life, with a wide range of reversible reduction/oxidation (redox) reactions. Its specific capacitance has been measured at 500 to over 750 F/g. [6] Unfortunately, it is also rare and very expensive.

Vanadium is a transition metal with lower conductivity than ruthenium, but with oxidation states from 5^+ to 1^- enabling many redox reactions; and it is abundant and cheap by comparison. Vanadium flow batteries are already in commercial use for solar energy storage.

Vanadium is usually found in nature in combination with other elements in their ores. In the earth's crust it is the 19^{th} most abundant element and the 5^{th} most abundant transition metal. The major suppliers of vanadium from minerals are South Africa, Russia and China. Vanadium is also found in crude oil from Venezuela and Canada, and can be recovered from oil refinery slag. [7]

2.2.1. Vanadium Phases, General Discussion

"VOx" is used in this document as a generic term for vanadium oxide in which the precise compound is not known or required.

Vanadium oxides are enormously complicated. Phases, states and morphologies shift with small changes in % oxygen, % water, pH, concentration, temperature and

applied voltage. Often, colors change along with the oxidation state or phase. Some of Vanadium's most common forms and their oxidation states are listed in Table 2.

Table 2. Common forms of vanadium oxides and their oxidation states

Compound	Ion	Oxidation state
V_2O_5	VO_3^- or VO_2^+	5+
V_2O_4	VO^{2+}	4+
V_2O_3	V3+	3+
VO	V2+	2+

In aqueous solution, vanadium species change from one phase to another based on pH and/or concentration as shown in

Figure 6.[8] Each predominance diagram shown represents only one valence level. Vanadium species also undergo pH-dependent change in response to applied voltage as shown in Figure 7 [8]; Pourbaix diagrams such as these are specific to one concentration. In these both figures, areas shaded and/or marked with (c) are solid (condensed) species; precipitation out of solution occurs in these regions. Phase diagrams such as these were helpful in this study; although they were not composed for the same conditions as used in this study, they provided a starting point for XRD analysis.

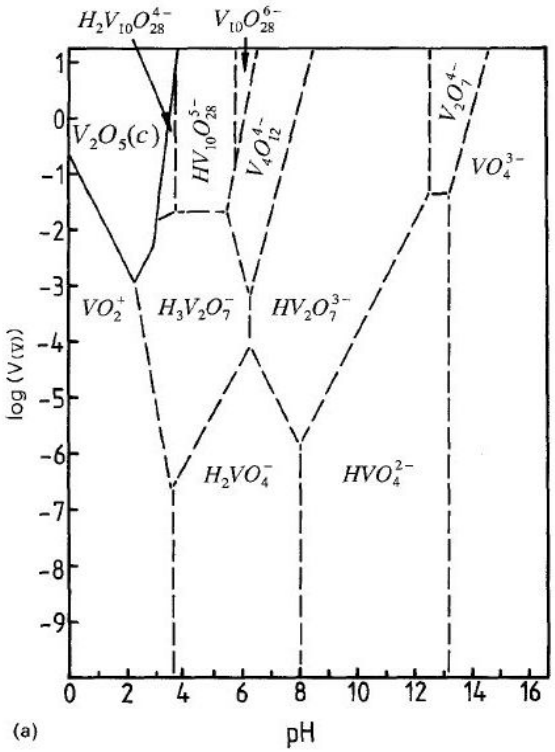

Valence 5^+, solid phase is V_2O_5

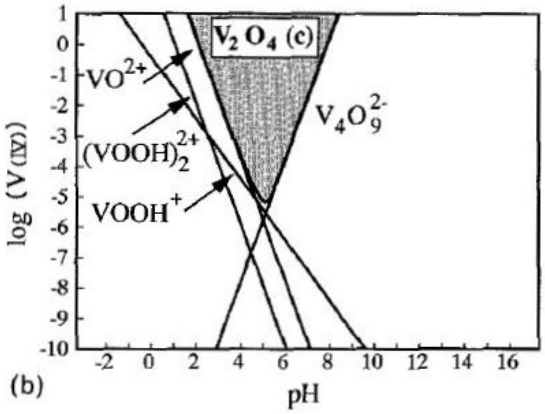

Valence 4^+, solid phase is V_2O_4

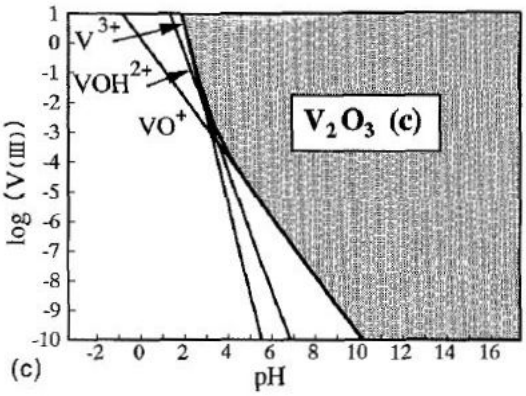

Valence 3^+, solid phase is V_2O_3

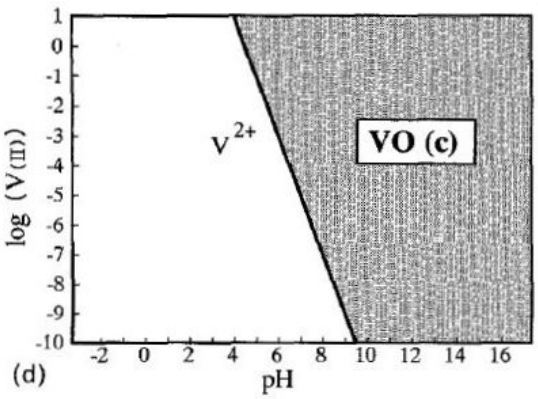

Valence 2^+, solid phase is VO

Figure 6. Predominance diagrams: concentration-pH phase diagrams at ambient temperature; shaded and (c) indicates solid (condensed) phases. Valences: (a) 5+, V(V); (b) 4+, V(IV); (c) 3+, V(III); (d) 2+, V(II). Figure copyrighted and reprinted from [8], Page 420, with kind permission from Springer Science and Business Media.

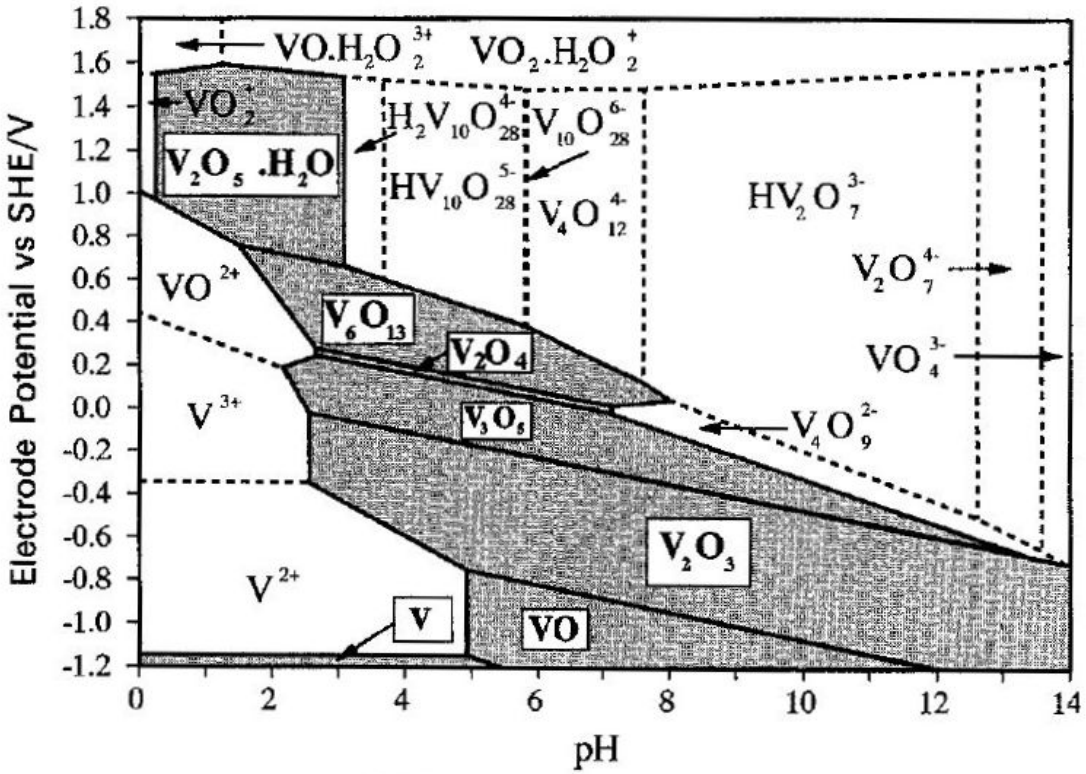

Figure 7. Pourbaix diagram, potential vs. pH, for the V-H_2O system; activity of dissolved vanadium species=0.01; valence state varies. Figure copyrighted and reprinted from [8], Page 419, with kind permission from Springer Science and Business Media.

2.2.2. Vanadium oxide basic structures

This section serves as background for the following sections which give brief descriptions of common VOx phases and morphologies.

Vanadium oxide compounds are comprised of basic units including tetrahedra as in VO_4, square pyramids or trigonal bipyramids as in VO_5, or octahedra as in VO_6, all of which join at corners or edges (see Figure 8). I.e., V atoms have coordination numbers of 4, 5 or 6. Vanadium oxides can contain more than one level of coordination, and the shapes can be distorted. Many vanadium compounds form long ribbons. These ribbons can weave into gels of varying porosity, or when crystallized can make nanorods or nanowires. Flakes or plates can also form. The configuration taken depends on

concentration, pH, amount of surface space and the energetic environment of the support site.

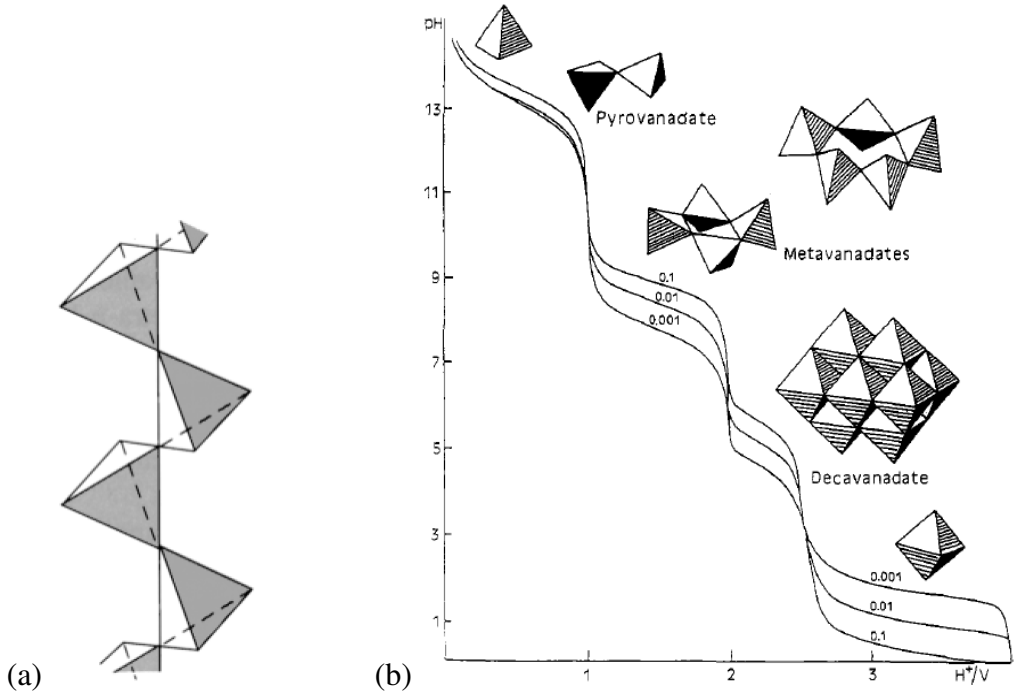

(a) (b)

Figure 8. Edge- and corner-sharing of vanadium oxide basic units: (a) VO_4 tetrahedra sharing corners; structure shown is NH_4VO_3 [7] p. 996. (b) Predominance of V(V) structures in aqueous solution based on pH, for three concentrations; .1M, .01M and .001M. Reprinted with permission from [9], Page 579. Copyright 1991 American Chemical Society.

H_2O can reside in oxide complexes between layers [10] as illustrated in Figure 11a , bridging as shown in Figure 9, or within the lattice (not shown). Figure 9 shows water molecules binding together vanadium complexes to form larger assemblies. As a point of interest, the complex shown in Figure 9a is of mixed valence V(V)/V(IV). [11]

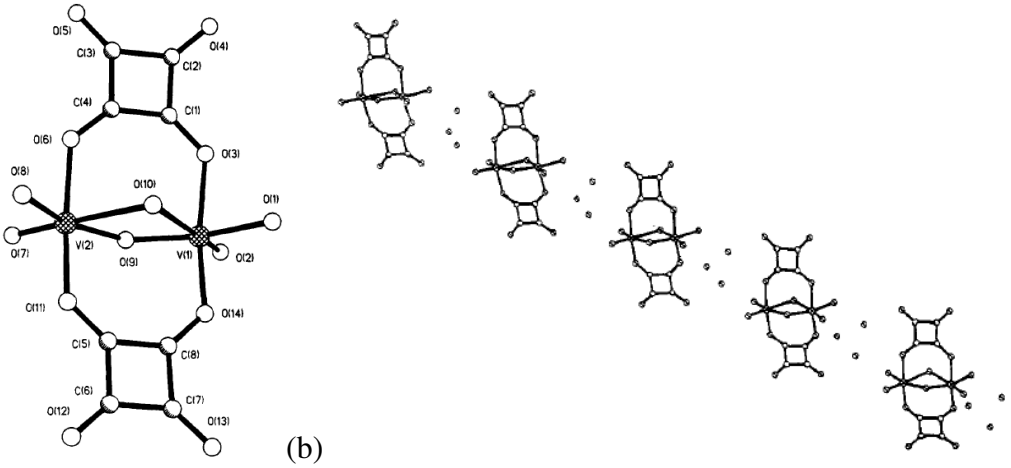

(a) (b)

Figure 9. Example of a mixed-valent (V)/(IV) complex; $[V_2O_3(C_4O_4)_2\text{-}(H_2O)_3]^-$. (a) The complex; (b) three water molecules between two complexes, all together forming a chain. Reprinted with permission from [11], Pages 6346 and 6348. Copyright 1994 American Chemical Society.

The first features to form over a support are small monomers and dimers such as shown in Figure 10; over the first layer, larger assemblies can form.

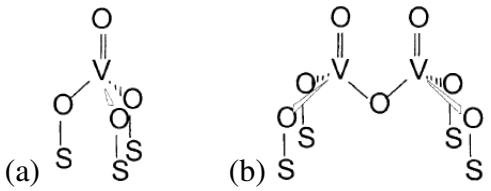

Figure 10. Possible configurations for vanadium oxides on support S at low coverage: (a) monomeric, (b) dimeric. Reprinted from [12], Page 29, Copyright 2003, with permission from Elsevier.

Many vanadium oxides form layered structures such as shown in Figure 11. These structures can be expressed in morphology (depending on processing) as nanowires and nanobelts formed by many phases. Compounds with layered structures have been frequently studied for lithium intercalation.

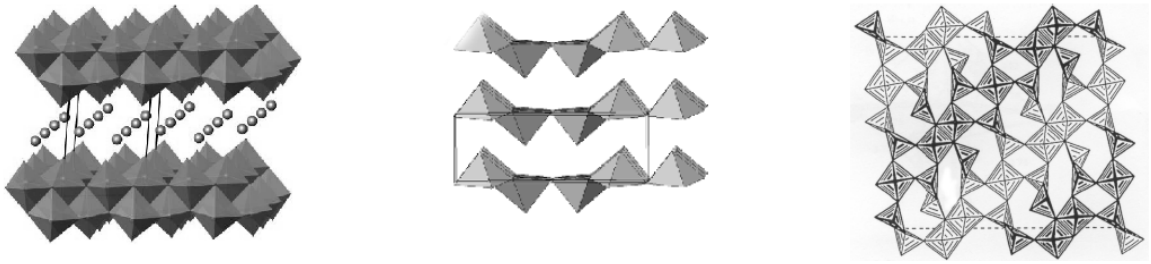

(a) (b) (c)

Figure 11. Model structures of (a) $(NH_4)_xV_2O_{5-\delta}$-nH_2O, (b) V_2O_5 and (c) V_3O_7. [13]

2.2.2.1. Water Content in Vanadium Oxide Phases

Water resides between layers and in the lattice itself as described in the previous section, and upon heating, water leaves in stages. The amount of water in a VOx phase can be quantified by thermogravimetric (TG) analysis.[14] An example of the water removal process follows for V_2O_5. Researchers are not in complete agreement about the details, but the sequence is as follows:

- V_2O_5 air-dries to V_2O_5-$1.6H_2O$ ([15], [16], [17]) or V_2O_5-$1.8H_2O$ [9]. At this point about 1 H_2O per V_2O_5 resides loosely bound between layers. [17]
- Interlayer H_2O leaves first up to 120°C, finishing at V_2O_5-$0.5H_2O$.
- Up to 250°C, water loss is reversible, and the material can easily reincorporate H_2O. [10]
- Between 250°C and 320-350°C, H_2O is lost from the lattice, ending in V_2O_5-$0.1H_2O$. [16], [17]
- At 350°C, V_2O_5 crystallizes, becoming V_2O_5 Shcherbinaite with orthorhombic structure.

  This process can be summarized as follows: [17]

$$V_2O_5\text{-}1.6H_2O \underset{120°C}{\leftrightarrow} V_2O_5\text{-}0.5H_2O \underset{250°C}{\rightarrow} V_2O_5\text{-}0.1H_2O \underset{320°C}{\rightarrow} V_2O_5 \text{ orthorhombic} \quad (7)$$

A simpler and slightly different theory: [9],

$$V_2O_5\text{-}1.8H_2O \leftrightarrow V_2O_5\text{-}0.5H_2O \rightarrow V_2O_5 \text{ amorphous} \rightarrow V_2O_5 \text{ orthorhombic} \quad (8)$$
$$\text{120°C} \qquad \text{250°C} \qquad \text{320°C}$$

The amount of water present between layers affects XRD patterns. For example, in V_2O_5, each layer of water corresponds to about 2.8Å. [9] Changes in interlayer distance result in shifted XRD degrees 2θ (from Braggs' law).

Thermogravimetric Analysis (TG) is sometimes used to study a material's mass response as heat is steadily increased; in the case of V_2O_5, mass loss indicates water removal. Figure 12 shows a Thermogravimetric and Differential Temperature Analysis (TG / DTA) performed on both amorphous V_2O_5 and a mixture of V_2O_5 with activated carbon. As predicted in equations 7 and 8, the The 'easy' water was removed up to 120°C, and carbon combustion began above around 330°C.

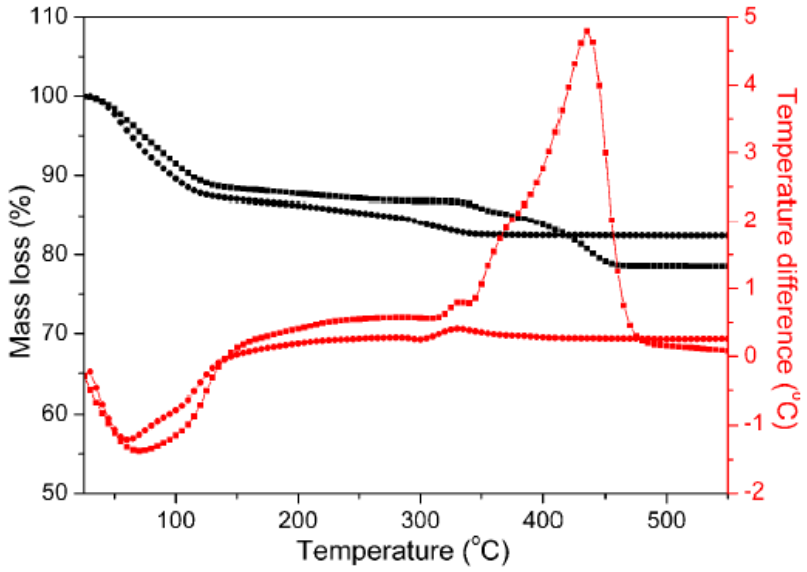

Figure 12. TG (black) and DTA(red) of air-dried (●)V_2O_5 and (■) V_2O_5 + 10wt% C. [18]

2.2.3. Highlights of a few common vanadium oxide phases and morphologies

Vanadium oxides can assume many forms and incorporate a wide range of O, H and H_2O. This results in many named compounds. Included herein are a few phases likely to be seen in this work.

2.2.3.1. Ribbons and Gels

Many amorphous vanadium oxides tend to form ribbons, which interlock and overlay to form gels. Amorphous V_2O_5 is one of the more commonly studied oxides in these forms. Figure 13 shows the modeled cross-section structure of a ribbon, and Figure 14 shows an SEM image of a typical gel. The degree of porosity determines whether the gel is termed (from low to high porosity) xerogel, ambigel or aerogel.

Figure 13. Cross section of a V_2O_5 xerogel ribbon. Several fibers (width 27 Å) join edge-to-edge to form the ribbon. The ribbons are corrugated in the c direction; length varies in the b direction. Reprinted from [16], Page 86, Copyright 1983, with permission from Elsevier.

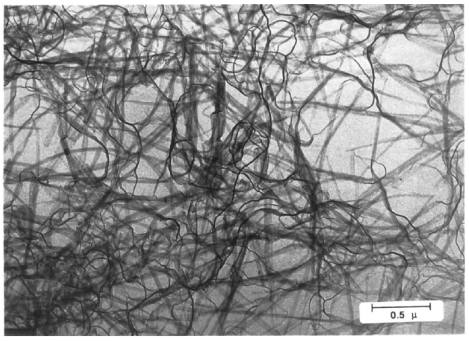

Figure 14. Fibrous structure typical of vanadium pentoxide gels. Reprinted with permission from [9], Page 581. Copyright 1991 American Chemical Society.

The evenness and size of pores varies with drying conditions; ambient drying results in small pores inhomogeneously distributed (xerogels) and supercritical drying results in a homogenous distribution of large pores (aerogels).[19] V_2O_5 gels have shown promise as pseudocapacitors, especially aerogels. In this study only the less-porous structures, i.e. xerogels, were expected. [15].

2.2.3.2. Nanobelts and Nanowires

Nanobelts and nanowires can be formed under many conditions from many precursors. Theories of formation include ribbons joining edge to edge, or layers defoliating and splitting lengthwise; however, the precise mechanisms are not relevant to this study. Figure 15 shows some examples of typical nanobelt morphology.

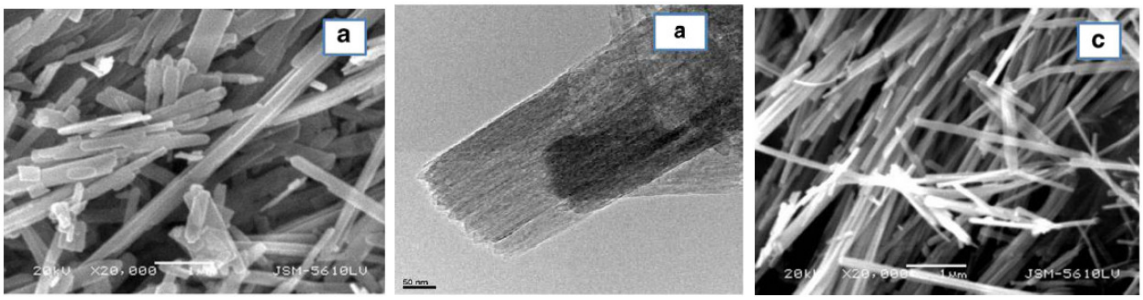

Figure 15. (Left) SEM of VO_2(B) nanobelts; (Middle) TEM of VO_2(B) nanobelts; (Right) SEM of V_3O_7 nanobelts. Scale bars 1µm, 50nm and 1µm respectively. Reprinted from [20], Page 612, Copyright 2012, with kind permission from Springer Science and Business Media.

2.2.3.3. V_2O_5 Crystalline

Much work in the Li-based study of vanadium oxides compares amorphous V_2O_5 gels to crystalline V_2O_5.

Crystalline V_2O_5, in mineral form known as shcherbinaite, is a common form of vanadium oxide which can be bought, or produced by many methods. It has a layered

structure showed edge-on in Figure 11b. Figure 16 shows nanobelt morphology commonly found in crystalline V_2O_5 resulting from hydrothermal treatment. [21]

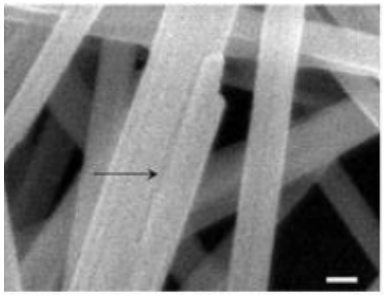
Scale bar: 100nm

Figure 16. V_2O_5 crystalline nanobelts, hydrothermal treatment 180°C 48 hr. Reprinted with permission from [21], Page 9384. Copyright 2006 American Chemical Society.

When V_2O_5 crystallizes in nanoshapes, its pseudocapacitance is enhanced.[22] Figure 17 shows an SEM of nanocrystalline V_2O_5. [23]

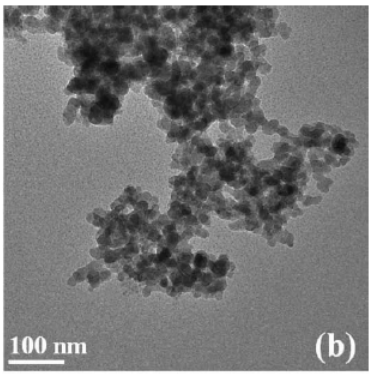

Figure 17. Nanocrystalline V_2O_5 resulting from annealing bariandite at 400°C. Reprinted from [23], Page 590, Copyright 2009, with permission from Elsevier.

2.2.3.4. Mixed Valence V_3O_7 and $H_2V_3O_8$

V_3O_7 is a mixed-valence compound, of layered structure shown in Figure 11c. The hydrated form, V_3O_7-H_2O, is known more recently as $H_2V_3O_8$. The mixed valence is accomplished by a combination of one VO_5 (valence 4) and two VO_6 (valence 5). [24], [25]. Of interest in this study are not the particular V atom arrangements, but the mixed

valence and the layered-structure morphology. Reference [25] contains a good image of the structure of $H_2V_3O_8$. SEM and XRD of these compounds can be found in references [25] and [26]. The electrochemical performance of nanostructured V_3O_7 has been shown to be approximately equal to that of VO_2(B) nanostructures and V_3O_7 is considered to show promise for lithium battery cathodes. [26]

2.2.3.5. Compounds with Oxalic Acid: Vanadium Oxalates

Oxalates, containing $[C_2O_4]^{2-}$, are possible intermediate compounds when oxalic acid is used with NH_4VO_3 or V_2O_5 precursors. Upon heating, oxalates change to other compounds such as V_2O_5. In [22] this began at 267°C and was complete by 292°C according to thermogravimetric analysis. Oxalates have been shown to be useful in creating nanoparticle morphology.[22, 27] As far as found during this study, oxalates have not been tested on their own in pseudocapacitance; they are always heated or reacted to form the final compound which is then tested.

2.3. Vanadium in Pseudocapacitance Studies

Vanadium oxides have been extensively studied in relation to Lithium batteries and intercalation, reporting performance in units of specific capacity (mAh/g). For this application, layered structures such as those found in amorphous V_2O_5 have superior performance over crystalline structures. However, work focusing on pseudocapacitance without lithium is less often published. As described in section 2.1.2, pseudocapacitance can involve surface or near-surface charge storage mechanisms in addition to slower intercalation used by the lithium ion.

Table 3 represents a sampling of research focusing on vanadium's pseudocapacitance. Phases of vanadium which have been shown to have good specific

capacitance include V_2O_5 (nano-featured or not crystallized), mixed-valence V_3O_7 and lower-valence VO_2.

Table 3. Electrochemical studies related to vanadium oxides.

Precursors	Resulting Phase	Highest Performance	Ref
V_2O_5 alone, quenched	amorphous V_2O_5, no peaks	350 F/g	[28]
NH_4VO_3, ethanol	V_3O_7	.23 F/cm^2	[29]
NH_4VO_3, HCl, surfactant	V_2O_5	388 F/g	[30]
$NaVO_3$, H_2SO_4	V_2O_5	225 F/g	[31]
$NaVO_3$, two resins	V_2O_5	214 F/g	[32]
$VOSO_4$	V_2O_5-xH_2O	910 F/g	[33]
$VOSO_4$, H_2O_2	VOx-nH_2O + V_2O_5-1.6H_2O + V_6O_{13}	185 F/g	[34]
VCl_3, NH_4OH	V_2O_5 Shcherbinaite	260 F/g	[35]
$C_9H_{21}O_4V$(V), acetone	V_2O_5 aerogel	2300 F/g	[36]
V_2O_5, water	V_2O_5 tetragonal	300 mAh/g	[37]
V_2O_5, water, glucose	V_3O_7-H_2O, VO_2(B)	296-227 mAh/g	[26]
V_2O_5, H_2O_2 10%	V_2O_5 amorphous until 330°C	123 mAh/g	[18]
NH_4VO_3, oxalic acid	VO_2(B) monoclinic	180 mAh/g	[38]
V_2O_5, oxalic acid	V_2O_5 nanoparticles	200-260 mAh/g	[22]

Following are highlights from studies of relevance to this work.

2.3.1. Enhancing vanadium oxides by coating onto carbon

Often vanadium oxides are combined with carbon to improve conductivity and electrochemical performance. Vanadium is less conductive than ruthenium and benefits from this treatment. The carbon does not form chemical compounds with the oxides; rather, researchers attempt to form an oxide coating over the carbon, with the goal of easing the path of electrons through the electrode.

Catalyst research provided some guidance about carbon-coating. A carbon-activation patent for purposes of capturing sulfur [39] pointed out that for good catalytic action, the coal must first be steam-treated (i.e., activated) and then impregnated with

vanadium, not the reverse. This is logical and pseudocapacitance studies follow this sequence; for example, by mixing vanadium oxides with activated carbon.

Also in [39], ammonium vanadate was recommended over vanadium pentoxide; NH_4VO_3 could be more easily mixed in water or oxalic acid, more quickly dried, and more safely handled than V_2O_5 in sulfuric acid. This helps both reduce cost and improve safety.

This patent and many other catalyst-fabricators soaked carbon in solution. However, soaking carbon in an oxide solution results in loading which is hard to predict because loading varies with time, pH, concentration and other factors. In [40], molybdenum oxides with acid pH tended to quickly form a crust while those with neutral pH slowly distributed evenly into the foam. This relates to a concept called "point of zero charge" which is beyond the scope of this document and this study; but the reader can pursue this topic further if interested.[41] Suffice it to say that the pH of both the solution and the carbon surface (as a result of pre-treatment) influences the amount and distribution of loading when soaking carbon.

In [42], Nanoscale vanadium oxides were loaded into carbon nano-tube-in-tubes via capillary action followed by drying and heating; the vanadium particles were small and well-dispersed (Figure 18). The precursors were ammonium vanadate and oxalic acid in a molar ratio of 2.1M : 4.2M. The loading was approximately 80wt% V_2O_5 and the authors reported favorable electrochemical results with Lithium; 90 $mAhg^{-1}$ and higher. [42]

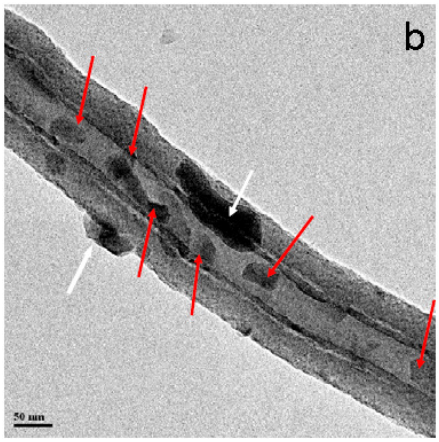

Figure 18. TEM image of V_2O_5 nanoparticles in carbon nanotube-in-tube. Particles inside are shown by red arrows; particles outside are shown by white arrows. Scale bar is 50nm. Reprinted from [42], Figure S3, Supporting Information, Copyright 2009, with permission from Wiley-VCH 2008.

The XRD of the V_2O_5-carbon nanotube-in-tube composite is shown in Figure 19. The composite was first heated to 400°C for 2hr. It was identified as crystalline orthorhombic V_2O_5 with estimated crystallite size about 30nm.

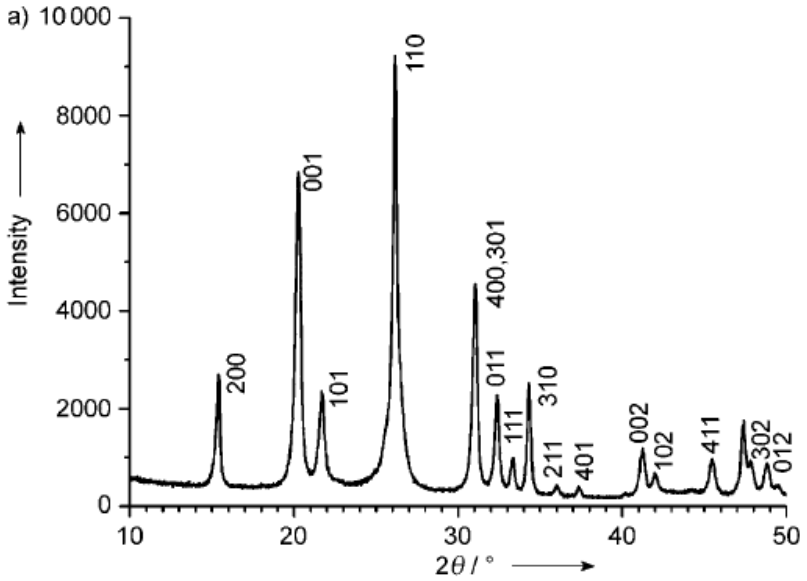

Figure 19. XRD of V_2O_5 nanoparticles in carbon nanotube-in-tube. Reprinted from [42], Page 211, Copyright 2009, with permission from Wiley-VCH 2008.

2.3.2. Carbon-enhanced xerogel compared with V_2O_5 alone

Often carbon is simply mixed in with the oxide. For example, Stojkovic et al. formed an amorphous-appearing gel from V_2O_5 solution, air-dried then dried further at 200°C for one hour: (a) alone, (b) carbon black mixed into the solution, and (c) alone heated to 330°C. The dried but un-annealed composite (b) had specific capacity of 123 mAh/g, more than twice that of the crystalline V_2O_5 (c, 63 mAh/g) or dried un-annealed pure gel (a, 50 mAh/g). [18]

2.3.3. Thin Films

A thin film study showed how morphology changed with increasing levels of annealing. V_2O_5 Films annealed at 250°C were smooth; those annealed at 300°C had nanoparticles and pores, and the maximum specific capacitance for this study; those annealed at 350°C and 400°C formed spherical particles and had lower specific capacity. The morphologies are shown in Figure 20 and the electrochemical results are summarized in Table 4. [43] The article left unanswered questions, but still provided useful information. (The question: d resembles b more than c; was there a labeling error, or an order-disorder transition from b to c?) Useful information: 1) Pores present at 300°C were gone at higher temperatures. 2) The specific capacitance increased up to 300°C and then dropped. 3) The film was nearly flat at 250°C and very aggregated by 400°C.

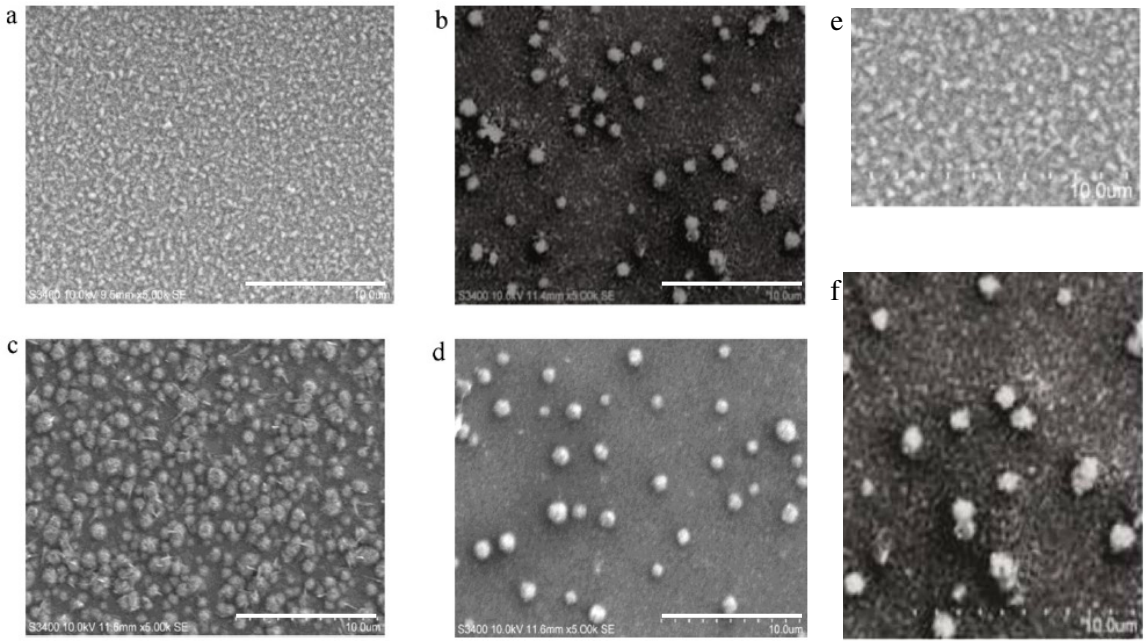

Figure 20. SEM showing aggregation of V_2O_5 films with annealing. All times 1 hour: a-250°C, b-300°C, c-350°C, d-400°C. Scale bar 10 µm. e- close-up of a; f-close-up of b. This figure and following table reprinted from [43], Pages 761 and 763, Copyright 2013, with permission from Elsevier.

Table 4. Characteristics of V_2O_5 films annealed at different temperatures. [43]

Variation of film parameters with annealing temperature.

Annealing temperature (°C)	Thickness (nm)	Grain size (nm)	Band gap (eV)	Specific capacitance ($F g^{-1}$)
250	177	Amorphous	2.40	241
300	202	26	2.36	346
350	212	48	2.29	226
400	224	68	2.22	177

2.3.4. Xerogels, and the presence of Nitrogen while annealing

Figure 21 shows aerogels formed from NH_4VO_3, from which NH_4^+ had been removed by ion exchange resin, but had N reintroduced during further processing. The gels after supercritical drying (under CO_2) had an XRD pattern identified as amorphous V_2O_5-1.6H_2O.

Figure 21a shows a gel aged six months before drying. Figure 21b shows the gel heated to 260°C for one hour; the gel broke down and it was identified as V_2O_5 crystallized shcherbinaite. Figure 21c shows the gel of (a) heated at or above 450°C, but under NH_3 so while the heat damaged the gel, nitrogen allowed it to retain some fibrous quality. This compound was identified as an oxynitride with valence ~3.4.

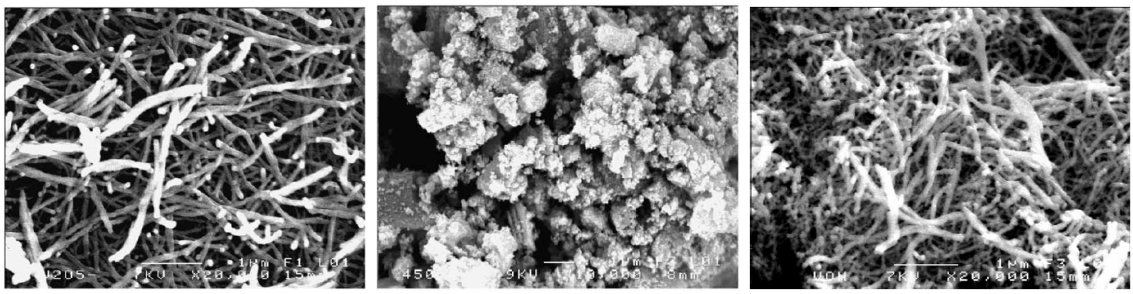

(a) (b) (c)

Figure 21. SEM of V_2O_5 xerogel:(a) as dried, V_2O_5-1.6H_2O; (b) heated at 260°C for 1 hr, V_2O_5 orthorhombic shcherbinaite; (c) oxynitride following calcining under NH_3. Scale bars 1µm. Reprinted from [44], Pages 220 and 222, Copyright 2005, with permission from Elsevier.

2.4. Carbon and Heat Treatment

Thermal treatment has been shown to effectively activate carbon without the use of hazardous nitric acid. From work by Skyllas-Kazacos et al., the thermogravimetric curve in Figure 22a shows carbon beginning to significantly lose mass (i.e., combust, releasing CO and CO_2) when annealed above 400°C. However, as activation temperature rose from 300 to 400, carbon's resistance reduced (Figure 22b). Wetting also improved dramatically when activated at or above 300°C; below this temperature it was hydrophobic. It was the theory of the authors that the heat treatment created C-O functional groups which enhanced hydrophilicity and interaction with vanadium ions. [45]

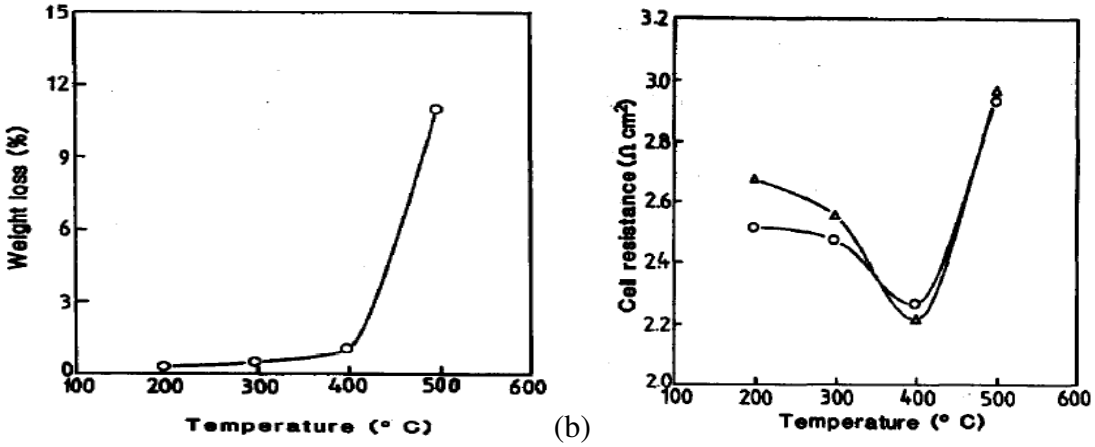

(a) (b)

Figure 22. (a) Graphite felt weight loss with activation temperature for 30hr. (b) Effect of activation temperature on resistance. Reprinted from [45], Pages 1259 and 1255, Copyright 1992, with permission from Elsevier.

2.5. Incipient Wetness Impregnation Method

Incipient Wetness impregnation differs from soaking or "wetness impregnation" in that the amount of solution administered to the support is equal to the pore volume in the support or slightly less. Capillary action spreads the active material evenly over the support. Catalyst supports are typically oxides with O-H groups which, upon heating, make a bond with the vanadium oxides as shown in Figure 23. [12] In the case of carbon supports, the carbon is activated to create these O-H groups.

The loading amount is linked to the solution concentration. The thinness and quality of coating (distribution, conformality) is related to surface area, pH of the solution and of the support surface, and functional groups. When higher loading is desired, the loading-drying process can be repeated. [12]

Figure 23. Incipient wetness impregnation process. Reprinted from [12], Page 33, Copyright 2003, with permission from Elsevier.

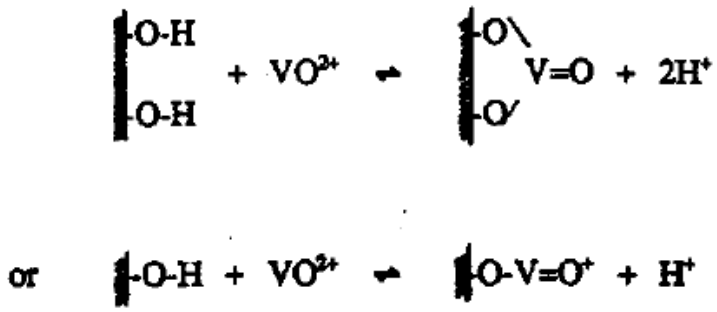

Figure 24. Vanadium ions binding to functional groups on carbon surface. Reprinted from [45], Page 1258, Copyright 1992, with permission from Elsevier.

Figure 24 above represents one way vanadium could bind to an activated carbon surface. Another possibility is as follows:[46] first, in acidic solution of pH < 2, the surface develops a positive charge:

$$\text{Support-OH} + H^+ \rightarrow (\text{Support-OH}_2)^+ \qquad (9)$$

Then the surface interacts with a negatively-charged ion, $[VO(C_2O_4)_2\text{-}H_2O]^{2-}$:

$$x(\text{Support-OH}_2)^+ + [VO(C_2O_4)_2\text{-}H_2O]^{2-} \rightarrow$$

$$(\text{Support-O})_x[VO(C_2O_4)_{2-x}] + xH_2C_2O_4 + H_2O \qquad (10)$$

2.6. Focus of this study

Vanadium oxides can be formed in many ways, including but not limited to: electrochemical deposition, atomic layer deposition, quenching from molten form, sol-gel, ion exchange resin, hydrothermal treatment, and chemical reaction. Vanadium oxide

electrodes are often fabricated by using a binder to hold vanadium oxides to carbon or other current collectors. Binder adds weight without electrochemical benefit.

This work represents a study of the pseudocapacitive performance of vanadium oxides made in a manner which was cost-effective and of minimal environmental impact. This means the process was to be simple and quick, requiring no special atmospheres, not involving days-long hydrothermal or aging, using inexpensive precursors and materials, and avoiding very hazardous chemicals. This work is an extension of that of others in our group, using binder-free methods to form the electrode material of interest onto inexpensive carbon fiber to enhance the current-carrying capability of the electrode.

This electrode configuration allows current to flow freely throughout the well-interconnected carbon backbone, ions to disperse freely through the wide spaces, and the oxide active material to interact directly between the two. The oxide coating should be thin and conductive enough that good current flows between the coated CFP and the cell connections, and coat the fibers evenly and thinly to make effective use of the active material.

The goals of this study, then, were as follows:

- Ideally, find a vanadium oxide with good electrochemical performance as a pseudocapacitor
- Coat evenly onto CFP without binder
- Use a simple process, avoiding very hazardous chemicals
- Test the effect of annealing
- Relate the performance to phase and morphology
- Define what procedures brought the material to the best-performing form

Performance would be measured and reported not in capacity (mAh/g) for Lithium batteries, but rather in capacitance (F/g or F/cm^2) for pseudocapacitor applications.

2.6.1. Choice of method to make pseudocapacitors

At the beginning of this study, a literature review was done, focusing on vanadium oxides as pseudocapacitors, and looking for nanoscale features, ease and quickness of fabrication, relatively safe precursor chemicals, combination with carbon, and of course good electrochemical performance.

Preliminary rounds of experiments were performed using the hydrothermal method with precursors V_2O_5 and oxalic acid, based primarily on reference [47] and our group's experience.[48] The results were: unremarkable electrochemical performance and carbon fiber coating which was uneven and difficult to control. Therefore, a second method was chosen.

This study used Incipient Wetness impregnation with single applications. For precursor solution, NH_4VO_3 was chosen. V_2O_5 is only slightly soluble in water, but NH_4VO_3 is more soluble in water, and even more so in oxalic acid. Oxalic acid assists in dissolution and reduces the vanadium. [12] NH_4VO_3 has been extensively studied as a catalyst precursor, and is often used via incipient wetness or by soaking to coat substrates. [49],[50]

CHAPTER 3: EXPERIMENTAL METHODS

3.1. Materials

3.1.1. Chemicals

Distilled water was obtained from Precision Water Systems' Precision Pure Model PWS 8-5, Series 0006. This model feeds steam through an activated charcoal filter. All references to water in this document refer to this distilled water unless specifically stated otherwise.

The precursors were ammonium vanadate (NH_4VO_3) purity unspecified by Fisher, oxalic acid ($H_2C_2O_4$) 98% by Aldrich, and ammonium hydroxide (NH_4OH) 28-30% by Aldrich. All chemicals were used "as is" without further purification.

Carbon fiber paper (CFP) was Spectracarb 2050L from Spectracorp, website www.eftspectracorp.com.

3.2. Synthesis of Vanadium Oxide electrodes

3.2.1. Basic Procedure

The basic procedure for fabricating vanadium oxide electrodes was as follows:

Ammonium vanadate (NH_4VO_3) and water were mixed in a 30ml sample vial, followed very shortly by oxalic acid powder ($H_2C_2O_4$), in amounts according to the desired concentration; in essence, the two were dissolved together. While stirring, the water bath was brought from room temperature or tepid to approximately 90°C. If no more dissolution was taking place, heat was raised on the water bath but boiling was avoided. The vial's lid was left askew at first under heat so gases could escape, but

closed relatively soon (when gas evolution seemed complete) and thereafter the lid was cracked slightly to vent every 5-15 minutes to release gases. After no further pressure difference was evident upon venting, the lid was left closed for longer periods. In this way the solution did not evaporate, but excessive pressure did not build up in the vial. Stirring continued for up to about 3 hours. If solids did not appear dissolved by this point, the vials were removed to a drawer; sometimes they finished dissolving overnight. This method was influenced by, in part, [42], [51], [49] and [50].

Portions of some samples were partly neutralized under stirring by the addition of ammonium hydroxide (NH_4OH) in the amount half-molar relative to the amount of vanadium.

A precise amount of vanadium solution was administered to prepared CFP by micropipette and the loaded CFP was left to air-dry overnight. The volume was intended to fill the CFP's empty space but not more. Based on data from the CFP vendor, the empty volume was calculated to be 77%. Some samples were further annealed at 250°C for three hours. Electrodes were punched from the resulting loaded CFP.

3.2.2. Carbon Fiber Paper (CFP) Cleaning and Pretreating

CFP was cleaned via ultrasound for five minutes in 1M sulfuric acid and five minutes in water, and rinsed with water before and after each step. Figure 25 shows SEM images of CFP before and after cleaning. The clean dry CFP was then annealed at 350°C for two hours to make it hydrophilic. Using thermal treatment to prepare the CFP achieved the goal of making it hydrophilic, without the use of nitric acid (commonly used to functionalize CFP). Figure 25b shows the clean CFP and Figure 26 shows the clean annealed CFP.

(a) 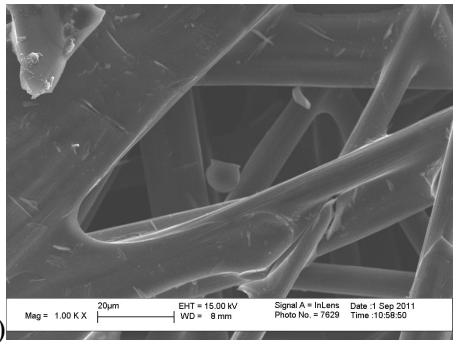

(b) 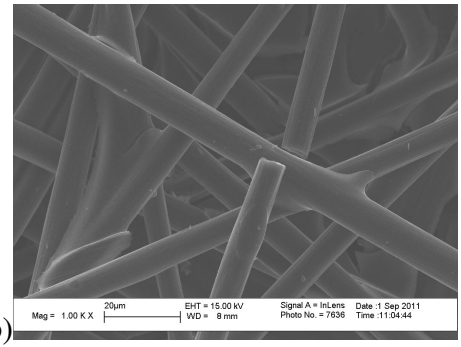

Figure 25. Carbon fiber paper (CFP) (a) before cleaning and (b) after cleaning.

(a) 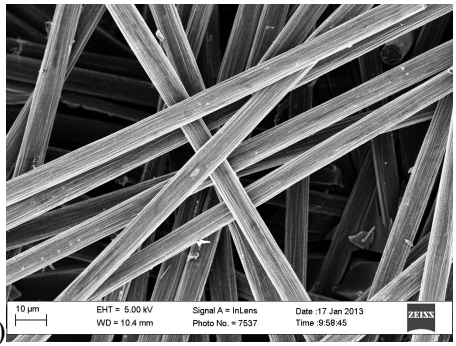

(b) 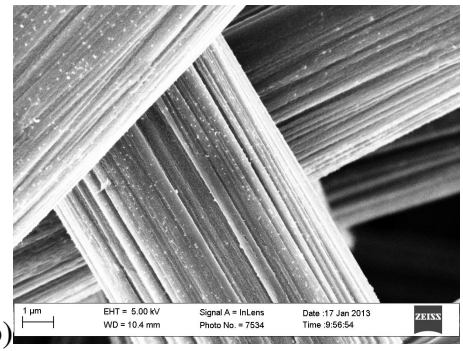

Figure 26. Cleaned CFP annealed at 350°C for two hours, magnification (a) 2kx and (b) 20kx.

3.3. Microscopic Characterization

X-Ray Diffraction (XRD) measurements were taken on a PanAlytical Alpha-1 with CuKα radiation, 4° starting angle, and .016 or smaller step sizes. The loaded CFP electrodes were measured using multiple scans and long times to differentiate any peaks from the amorphous carbon background. SEM images were obtained with a Leo 1530.

3.4. Electrochemical Characterization

3.4.1. Instrumentation and Configuration

Electrochemical measurements were performed via Schlumberger SI 1286 or Solartron 1285 electrochemical interface units using a two-electrode cell. The two-

electrode cell has the advantages of quick assembly and the ability to store it for later testing. In the two-electrode cell, both charge and discharge behavior is based on electrochemical characteristics of the active material. Although it does not provide a precisely-known voltage level as a three-electrode cell can, for oxide comparison purposes the two-electrode cell was considered suitable. [52], [53]

3.4.2. Cell Assembly

Symmetrical two-electrode cells were assembled from stainless Swagelok-type components. A polymer gasket and O-ring kept the two halves apart and the cell watertight. The separator was punched from a glass-fiber filter. Stainless steel disk spacers and spring washers provided contact from one side of the cell to the electrode; on the other side of the cell the electrode rested directly on the cell casing. A nylon "tube clamp" held all this together and compressed the cell. Copper adhesive tape provided the connection between the cell casing halves and the test leads. Figure 27 illustrates the cell assembly.

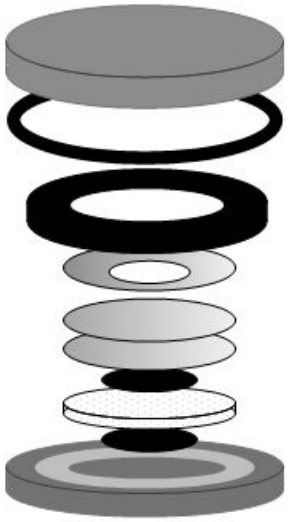

Figure 27. Swagelok-type two-electrode cell assembly.

Swagelok cell metal parts were lightly polished to remove oxides when needed, and then cleaned with water and ethanol. Enough electrolyte was added to moisten but not to saturate the separator (four drops).

3.4.3. Electrolyte

1M Na_2SO_4 was chosen as electrolyte because it has demonstrated adequate performance as an electrolyte for vanadium-based supercapacitors [54], it is environmentally benign, and was expected to be less likely to change the chemistry of the electrodes than other choices such as sulfuric acid or potassium hydroxide. It was also in use by others in our group for related work with which this work was intended to compare.

Since the electrolyte is aqueous, the voltage range of electrochemical testing was limited to 0.0-0.8V to avoid hydrolysis of water.

3.4.4. Loading

Areal loading in moles/cm^2 was calculated from solution concentration and volume applied, and loading in wt% was calculated from measured mass. Loading for purposes of calculating specific capacitance was calculated by subtracting the unloaded mass of the CFP from the air-dried loaded mass.

Our measurements showed that CFP mass can vary on average 8% between extremes of humidity. Therefore, a constant-humidity chamber was established in a glass desiccator, using sodium bromide (NaBr) saturated solution to maintain a relative humidity of 57%, which was close to the normal ambient humidity in our labs. Loaded and unloaded measurements could then be taken at the same humidity so the only difference was the coating.

During annealing, both CFP and active material lose mass, via different mechanisms. VO_x releases a significant amount of H_2O as described in section 2.2.2.1, and CFP releases CO or CO_2 as it begins to combust. These gases can act to reduce the overlaying vanadium oxide coating. Since substrate and coating do not necessarily lose the same amount relative to each other and there may be an interaction between carbon's functional groups (if any) and VOx, the % loading determined for annealed samples is not the same as if annealed VOx were applied to annealed CFP. However, since the annealing temperature was modest for carbon (250°C), it was not expected that the CFP would lose mass through combustion. It was expected that most of the mass loss would be from the VOx itself. Therefore, the annealed mass was used for annealed samples in F/g calculations.

CHAPTER 4: RESULTS

Following are the names used in this thesis as shorthand for the conditions of mixing and loading for the Incipient Wetness impregnation experiments which resulted in high specific capacitance. One lower-performing combination is also listed for comparison. All annealing was done at 250°C for three hours. All CFP were impregnated by pipette with 15.4 µL per cm^2.

Table 5. Solution details and names.

Name	Conc. of V (NH_4VO_3)	Conc. of oxalic acid (H_2C_2O4)	Ratio mol V : mol acid (H^+)	Conc. of neutralizing agent added (NH_4OH)	Solution approx. pH	Solution color
ConcA	2.1M	4.2 M	1 : 2	0	1.5	dk.blue
ConcN	2.1 M	4.2 M	1 : 2	1.05 M	2.0	dk.green
'A'	1 M	2M	1 : 2	0	2.0	dk.blue
	Mass ratio VOx:CFP unheated	Wt% unheated	Mass ratio VOx:CFP annealed	Wt% annealed		
ConcA	77%	44%	28%	22%		
ConcN	88%	47%	25%	20%		
'A'	32%	24%	2%	1.6%		

Lower concentrations were also attempted but quickly abandoned, as too little coating formed on the CFP and electrochemical performance was approximately the same as bare CFP. Citric acid was also tried and abandoned for the same reasons. A 1M version with no acid whatsoever was equally unremarkable.

4.1. Electrochemical performance

Electrochemical performance is reported first in this document because that was the first quality to be evaluated, prior to XRD or SEM. Samples with better specific capacitance were characterized further with XRD and SEM.

4.1.1. Calculations for Specific Capacitance

Specific capacitance was calculated based on the discharge slope of the galvanic cycle curves.

Capacitance (C) is defined in Farads, units [A·s/V]. This can be stated as

$$C = \left[\frac{A\ s}{V}\right] \quad \text{or} \quad C = \left[\frac{A}{V/s}\right] \quad \text{or} \quad C = \frac{I}{dV/dt} \qquad (11)$$

The last expression conveniently uses the applied current and discharge slope of the galvanic cycle curves. *I* was the applied current in A/cm^2 times one electrode area. Electrodes were 5/16" diameter, or .49483 cm^2. The slope of the discharge curve (dV/dt) was taken from the straight section below the IR drop if there was any.

The capacitance measured in a two-electrode symmetrical cell is the total capacitance, C_t. The two electrodes with separator and aqueous electrolyte between them act as two capacitors in series as illustrated in Figure 5b. In such a circuit, the capacitance of the electrodes is related to the total capacitance by:

$$1/C_t = 1/C_1 + 1/C_2 \qquad (12)$$

With identical electrodes in each half of the cell ($C_1 = C_2$),

$$1/C_t = 2/C_{electrode} \quad \text{or} \quad C_{electrode} = 2*C_t. \qquad (13)$$

Therefore, the capacitance calculated from measured values was multiplied by two and, to achieve specific capacitance, divided by the active mass of one electrode.

[53] For areal capacitance in F/cm^2, the capacitance was instead divided by the superficial area of one electrode.

4.1.1.1. Reporting Capacitance: F/g vs. F/cm^2

Specific capacity is more often reported in F/g of active material than in F/cm^2. Both units have their merits and drawbacks, and both are reported in this document. F/g can be skewed dramatically high by a very small mass, and F/cm^2 can have uncertainty of actual surface area. In the end, it is the overall cell's performance that matters.

For this study, units of F/cm^2, using superficial surface area, were the most convenient to compare one oxide to another, considering the wide variance in loading studied.

4.1.2. Electrochemical Test Results

Cyclic voltammetry and galvanic cycling experiments were performed on all samples.

4.1.2.1. Cyclic Voltammetry (CV) Profiles

Figure 28 gives an example of how CV profiles change with annealing. The enclosed area of the annealed-electrode's CV is larger than the unheated-electrode's CV, indicating a higher areal capacitance. Neither curve shows a specific redox peak.

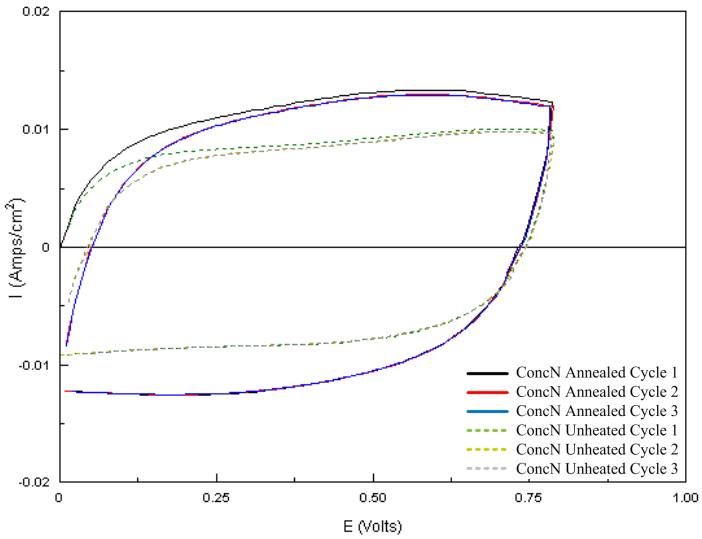

Figure 28. Cyclic voltammetry (CV) at 50 mV/s, three cycles each: solid line, ConcN annealed; dashed line, ConcN unheated.

The scan rate of 50mV/s was chosen to compare the CV scans of one sample with another. Figure 29 shows a comparison of the annealed samples with the highest areal capacitance (ConcA, ConcN). Bare CFP and a lower performer ('A') are shown for comparison.

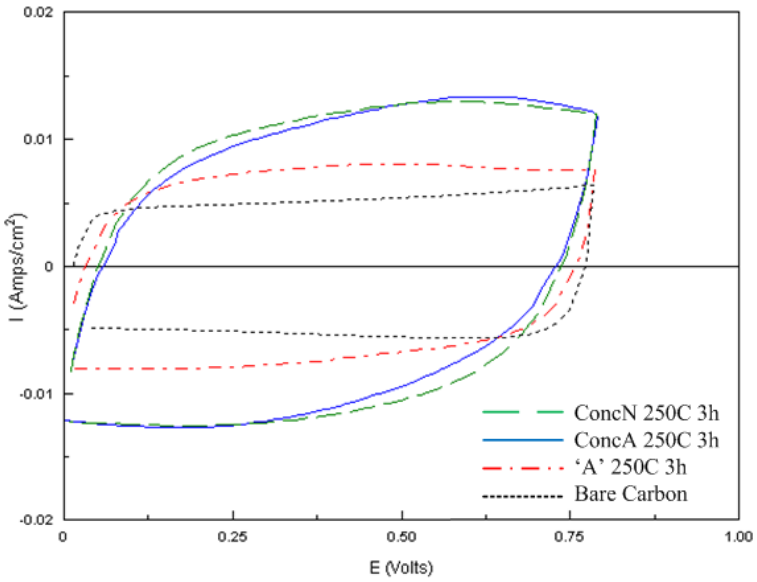

Figure 29. CV comparison at scan rate 50 mV/s of the samples with highest areal capacitance. Prepared bare carbon and a lower performer are shown for comparison.

The following figures show the CV at scan rates from 5-200 mV/s of the concentrated annealed samples, along with low concentration 'A' for comparison.

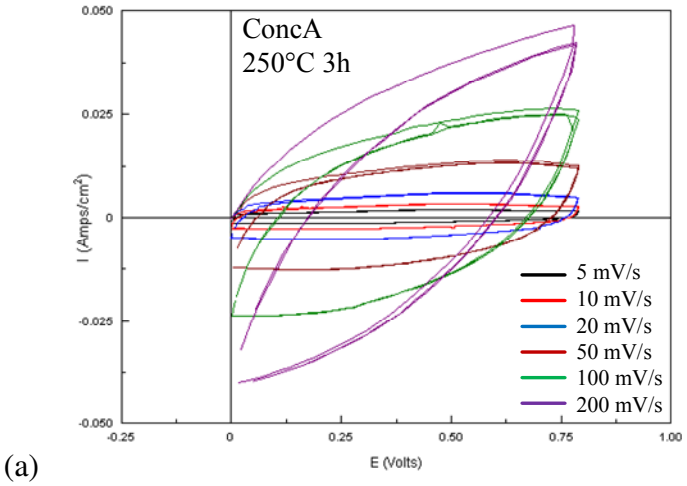

(a)

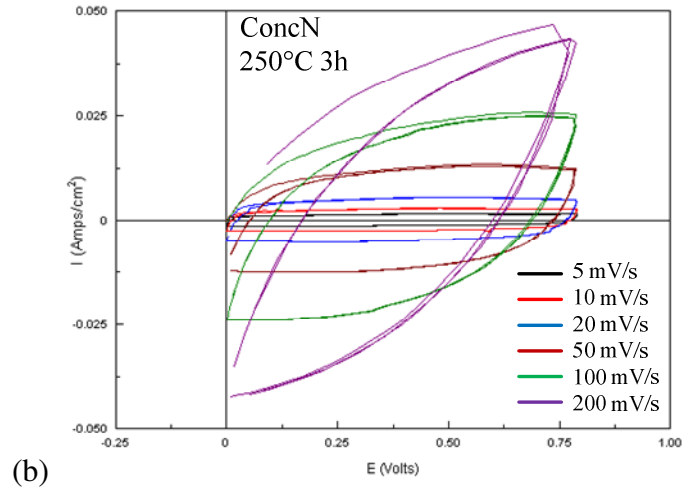

(b)

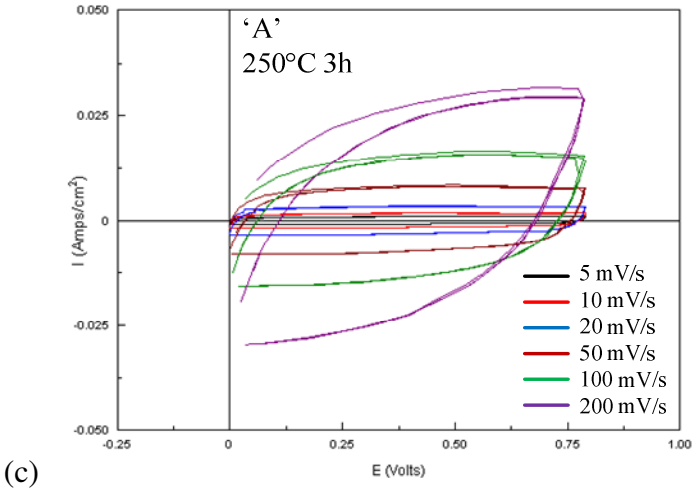

(c)

Figure 30. CV scans, 5-200 mV/s, 0.0-0.8V: all annealed 250°C 3h; (a) ConcA; (b) ConcN; (c) 'A'

The following can be observed from these CV:

- A completely straight, rectangular shape would indicate ideal capacitance with no losses, or an EDLC. Rounding of corners in these patterns indicates some internal resistance. The long humps in the rounded charge/discharge portions indicate pseudocapacitance.
- Symmetry indicates reversibility, and it can be seen that all are symmetric.
- The CV's of ConcN and ConcA are very similar.
- A fast drop-off at discharge indicates rapid response; ConcN has a slightly faster response than ConcA.
- Intercalation and other voltage-specific reduction-oxidation processes would have been indicated by peaks in the CV. No curve shows a redox peak.

4.1.2.2. Galvanic Cycle Profiles

Galvanic cycles were measured for 0-0.8V using 0.5-20 mA/cm^2. The galvanic cycle curves of prepared bare carbon are shown in Figure 31 for comparison with the data from the vanadium oxides in subsequent figures.

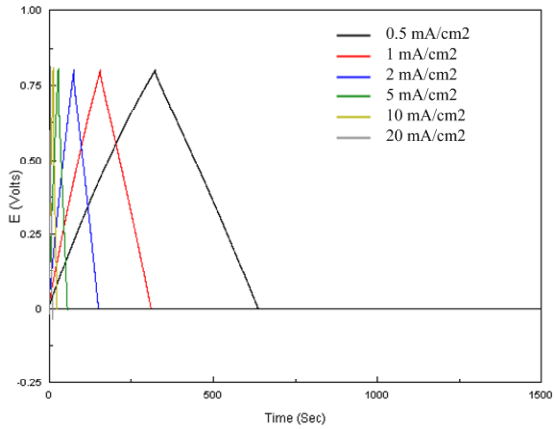

Figure 31. Galvanic cycles of bare carbon, cleaned and annealed at 350°C for 2 hours; i.e. prepared for loading.

Shown in Figure 32 are galvanic cycles for samples with high areal capacitance.

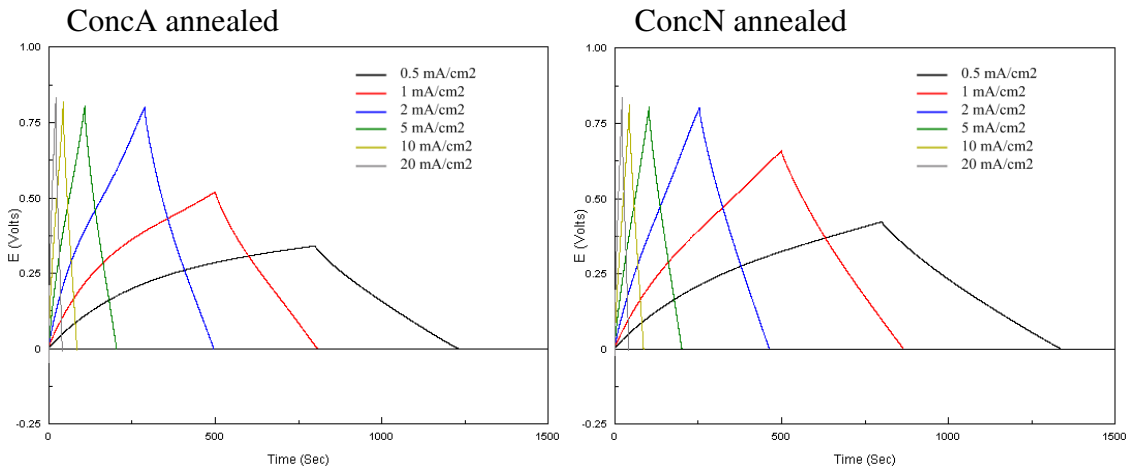

Figure 32. Galvanic cycles for (left) ConcA 250°C 3hr; (right) ConcN 250°C 3hr.

The reason the lowest scans did not reach 0.8V is that time limits were placed on the scans. The more-concentrated annealed samples reached the time limit before attaining maximum voltage. This could be an indication of a pseudocapacitive event such as intercalation, which only has time to happen during slow scan rates.

Figure 33 compares at a single scan rate (5 mA/cm^2) the galvanic cycles of these best performers with bare carbon, and also with a lower-performer.

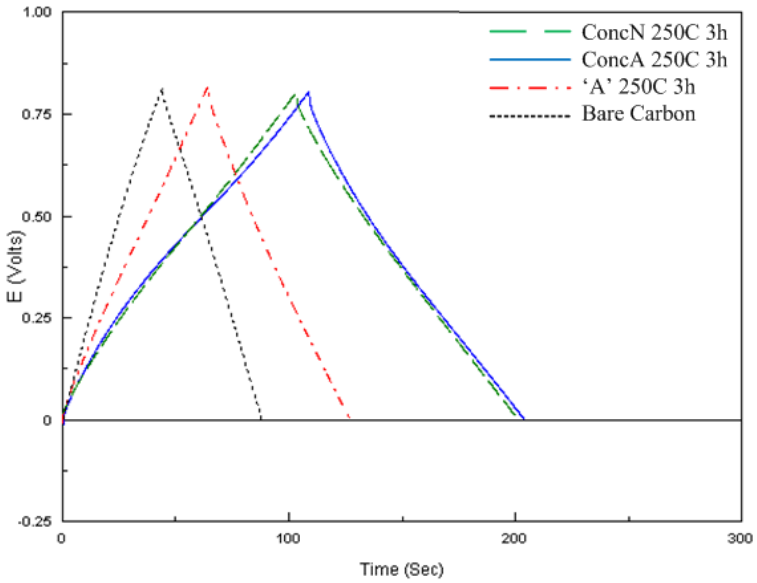

Figure 33. Galvanic cycles at 5 mA/cm^2 for ConcA, ConcN, 'A' (all annealed 250°C 3 hr), and bare carbon.

The following can be observed from the galvanic cycle curves:

- The long charge, not reaching 0.8V, could indicate intercalation.
- Long discharge, i.e. shallow slope, indicates higher specific capacitance.
- The IR drop at the beginning of discharge is very small, indicating that cell resistance is low.
- ConcA exhibits the curved shape of pseudocapacitance both in its charge and discharge. ConcN shows some curvature on the discharge.

4.1.3. Summary of Electrochemical Measurements

Figure 34 shows a selection of the highest specific capacitances measured in this work. The samples with highest specific capacitance were (annealed 250°C 3hr) ConcA and ConcN. A lower-performing sample and bare carbon are also included for comparison purposes.

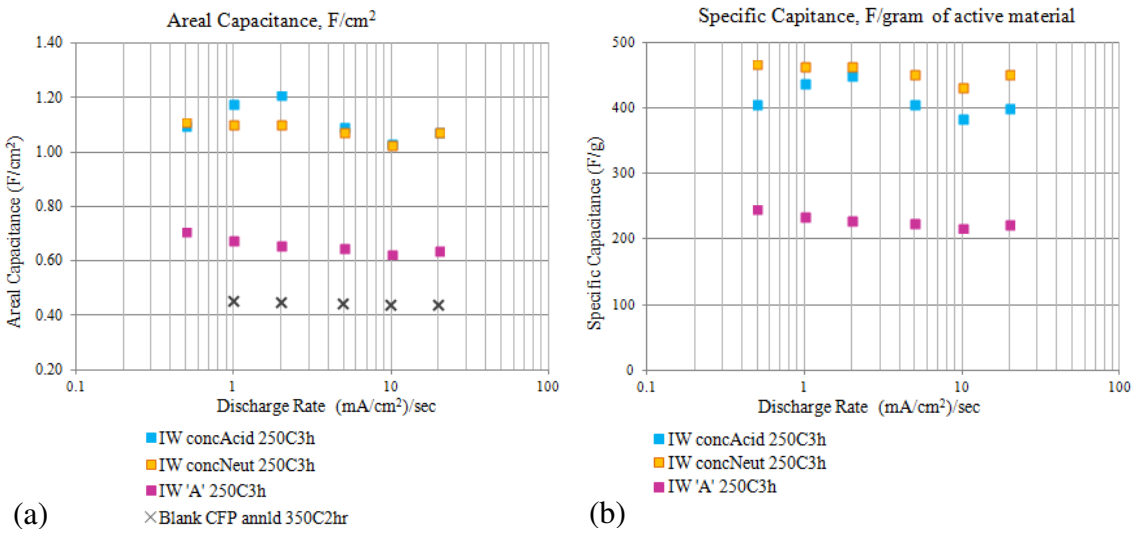

Figure 34. Capacitance of annealed samples: (a) Areal capacitance, F/cm^2 of electrode size; (b) Specific capacitance, F/g of active material.

In all cases, samples annealed at 250°C for three hours had better areal capacitance than un-annealed samples. This trend is illustrated in Figure 35.

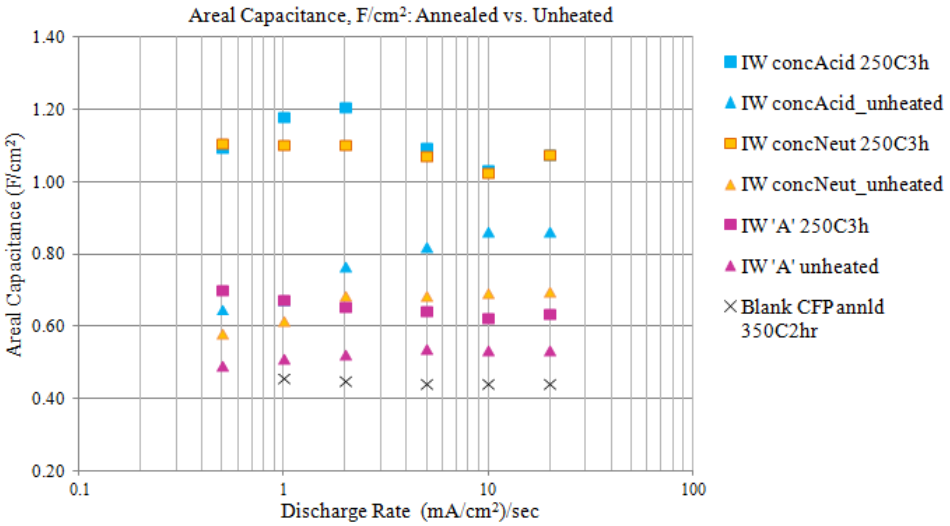

Figure 35. Areal capacitance for unheated and annealed samples; bare carbon shown for comparison. Annealed = squares; unannealed = triangles.

The effect of concentration can be considered in terms of loading. Figure 36 shows areal capacitance related to loading calculated from (a) loading calculated from

concentration and (b) derived from mass measurements. It can be seen that higher loading resulted in higher areal and specific capacitance.

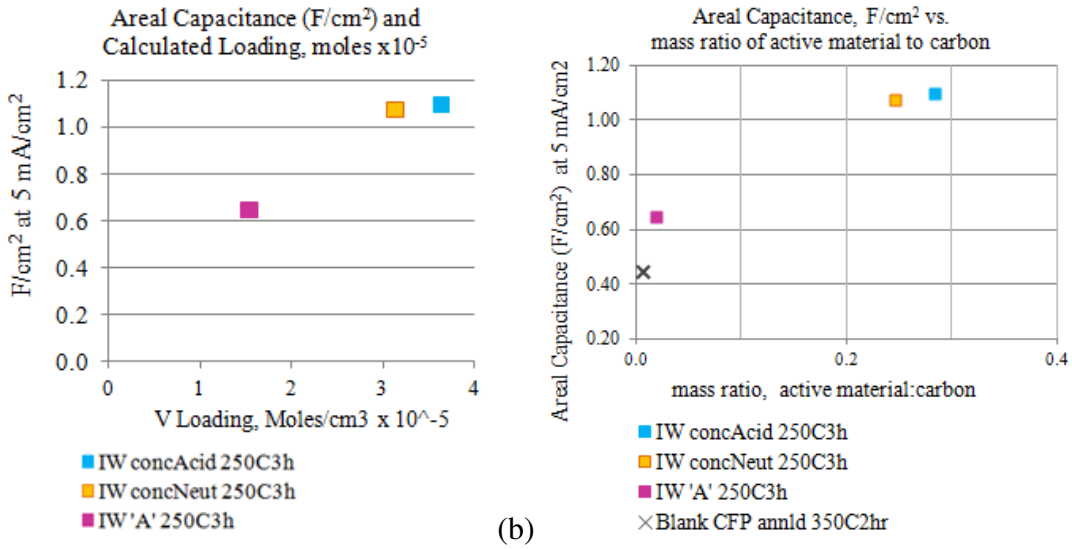

(a) (b)

Figure 36. Areal capacitance vs. loading: (a) calculated number of moles/cm^2; (b) by mass measurement, ratio of loaded (active) material to carbon.

4.2. X-Ray Diffraction (XRD) analysis

XRD was used to analyze the coated CFP electrode material. The reader is advised up front that phase determination by XRD could not be considered conclusive, because several phases were possible and no one stood out by itself; however, this work would be useful in guiding future characterization using other techniques.

The CFP itself was amorphous; no peaks were evident as shown in Figure 37, although the general profile followed Carbon (JCPDS 01-077-7164). Therefore, any peaks that arose could be assigned to vanadium phases. All VOx patterns followed the general shape of this CFP profile.

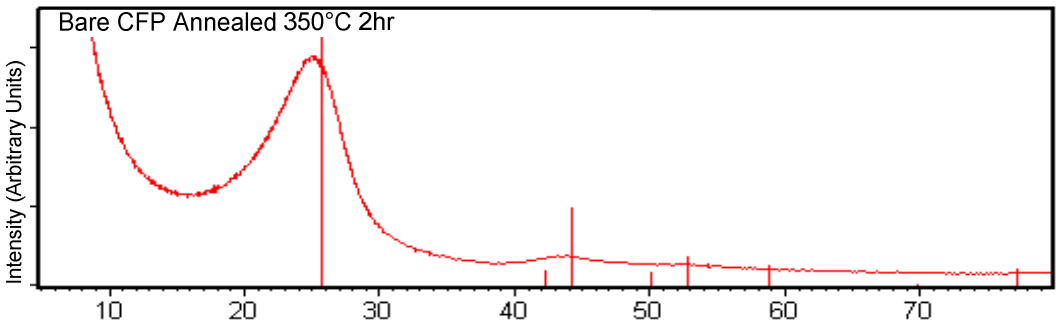

Figure 37. XRD of bare carbon annealed for 350°C 2hr along with reference pattern for carbon JCPDS 01-077-7164.

Figure 38 shows a typical un-annealed sample from the Incipient Wetness study along with the carbon profile. The lack of discernible peaks in the patterns of unheated samples indicates amorphous structure. Lines appearing as peak-beginnings at the top of the hump in the figure below are artifacts of computer-screen resolution; upon zooming in, one finds no humps or peaks.

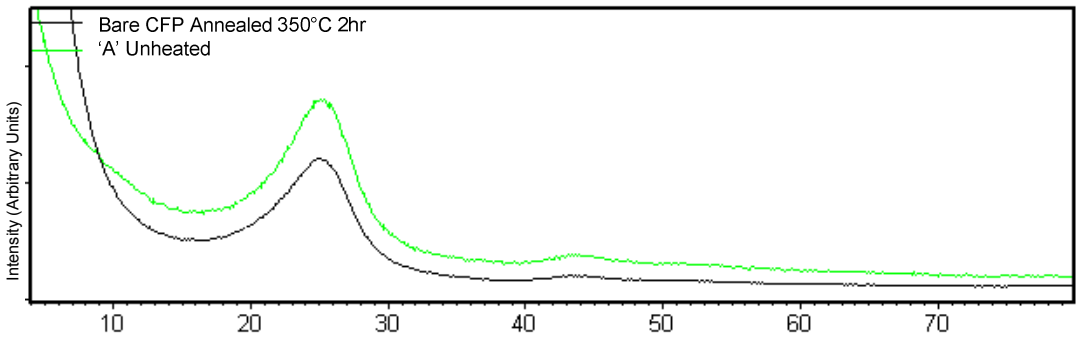

Figure 38. XRD of (green) incipient wetness unheated sample, 'A' shown; (black) bare carbon.

Figure 39 shows XRD patterns of samples annealed at 250°C for 3 hr. (Again, some of the jagged appearance of the lines is due to computer screen and printer artifacts; the lines smooth upon zooming in.) The peaks that began to develop were short and broad.

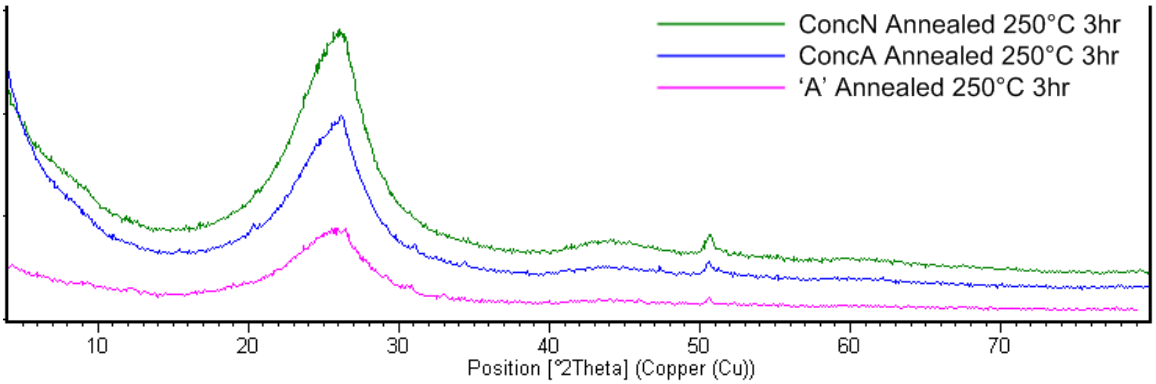

Figure 39. XRD of annealed samples: blue- ConcA, green- ConcN, fuchsia- 'A.'

Figure 40 highlights the differences in XRD patterns caused by the halving in concentration from 2M to 1M. It can be seen that the fully acidic solutions crystallized differently as a result of the reduced concentration, but the slightly neutralized solutions remained amorphous and very similar to each other in XRD.

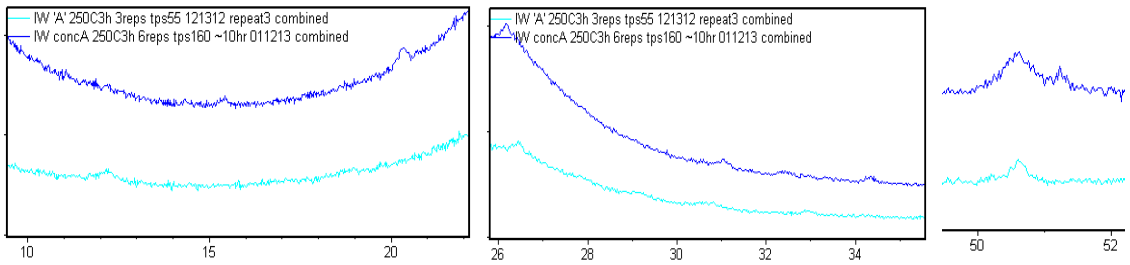

(a) Dark blue - ConcA, 2.1M; Light blue – 'A', 1M

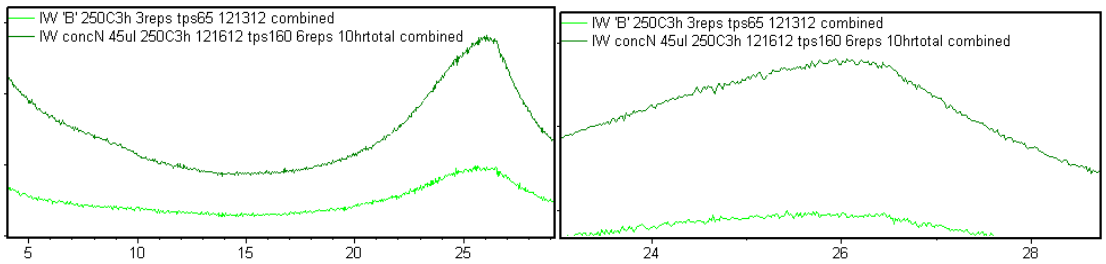

(b) Dark green - ConcN, 1.81M; Light green - 0.934M

Figure 40. Differences in XRD between annealed samples made from ~2M and ~1M concentrations of V. (a) Acidic; (b) slightly neutralized by addition of ammonia.

To summarize the similarities and differences in these three patterns:

- Two peaks ($2\theta \approx 26°$ and $\approx 50.6°$) are common to all the annealed samples, even amorphous ConcN. The phases matched with the definable peaks from the more crystallized patterns can therefore be extrapolated (using judgment) to the amorphous ConcN.
- An extra peak at ~51.2° is present in ConcA only.
- Comparing ConcA and 'A', peaks are shifted slightly or in different places, indicating that 'A' has different phases, or a different mix, rather than simply "less" of ConcA.

4.2.1. Guidance for Phase-Matching

The phase of VOx phase in solution varies with pH and concentration. Predominance diagrams ([55], [8]) such as those shown in section 2.2.1 served as a guide. For example, phases shown for pH <=2 were more likely than those shown for pH >2. However, these diagrams did not completely fit this study's parameters. First, only the top edges of the phase diagrams (or higher) were at all relevant due to the high concentrations of vanadium used in this study. Secondly, since the vanadium in solution was expected to be partly reduced by the oxalic acid, the condensed phases were expected to be valence-intermediates of those shown in the V(V) and V(IV) diagrams in section 2.2.1. The chemistry of vanadium oxides is complicated and many intermediate phases exist.

To relate this study's data to the predominance diagrams, Mol/cm^2 loading was calculated based on solution concentration, dosage and CFP surface area. For samples in which a half-amount of ammonium hydroxide was added to neutralize, the molarity was adjusted to account for the extra liquid. These values are shown in Table 6.

Table 6. Solution concentrations and pH.

Name	Ratio moles of V : moles acid :moles base	[V], M	Log(M)	Solution approx. pH	Moles V per cm^2 of CFP x10^{-5}
ConcA	1 : 2 : 0	2.1	0.32	1.5	3.2
ConcN	1 : 2 : 0.5	1.81	0.257	2.0	2.8
'A'	1 : 2 : 0	1	0.0	2.0	1.5

4.2.2. Matching to reference patterns

All samples annealed at 250°C for 3 hours shared two major features: a high point around 26° 2θ and a peak around 50.5°. The approach taken in phase-seeking was to match first these two major peaks; then to further differentiate between ConcA and 'A' to find which phase(s) might have influenced ConcA's better electrochemical performance.

Aside from the two main high points around 26° and 50.5°, and even on them, the peaks were quite small, sometimes only a suggestion above the background. Assigning a phase to ConcN was difficult because between 25° and 27° were many tiny peaks, all of which may have been equally relevant; and aside from these and the peak at 50.6°, ConcN was amorphous. The most distinguishable features in ConcA were a focusing of the large hump to a sharper peak at 26.2°, a small peak at 51.2° and a short broad peak at ~20.3°. The most distinguishable features in 'A' were the change in shape and shift at 26 to 26.45°, and a short broad peak around 12.2°. Both ConcA and 'A' had other minor peaks, or suggestions thereof, in the range from 29°-47°.

No single phase matched all of the major and small peaks. For every peak, multiple possibilities matched in a variety of valences and phases. All of these phases were considered to be within the realm of possibility. In short, phases could not be assigned with certainty.

For ease of comparison, the background has been subtracted in the patterns to follow. Matches to reference patterns from the JCPDS database are shown first by category, then put together.

4.2.2.1. V_2O_5

V_2O_5 was expected as a possible phase if some of the precursors remained at valence 5+; V_2O_5 would be predicted from the predominance diagrams due to the pH and concentration. Figure 41 shows how V_2O_5 reference patterns matched this study's data; the legend follows in Table 7 below the figure.

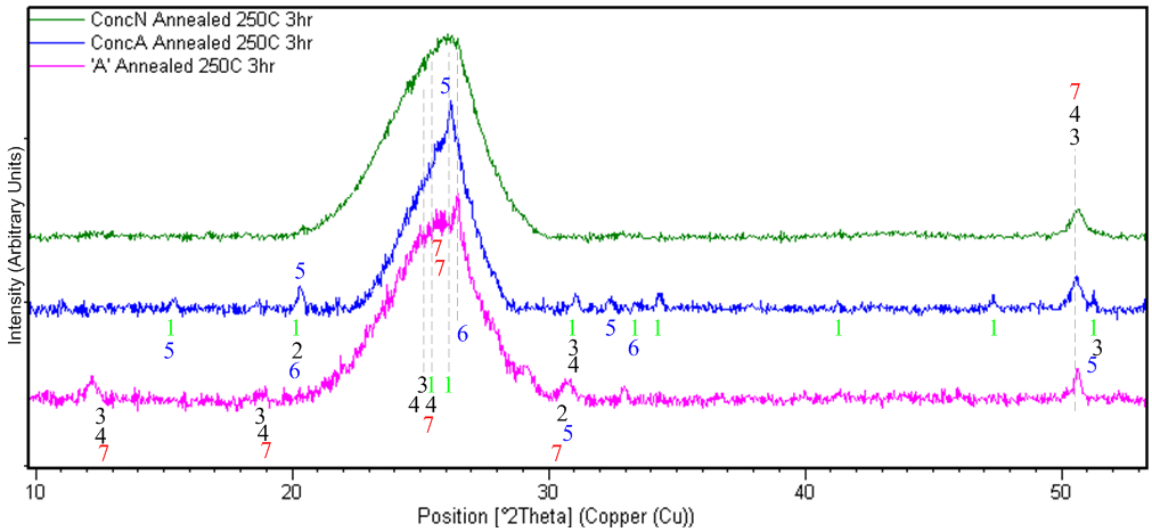

Figure 41. XRD, Annealed samples with background subtracted: Overlaid with matches to V_2O_5 reference patterns. Green- crystalline; Black- other, valence 5; Blue- reduced valence; Red- containing ammonium ion (NH_4^+) (also reduced valence).

Table 7. Legend for V_2O_5 XRD Reference Patterns.

#	Name	Valence	JCPDS Ref #
1	V_2O_5 shcherbinaite	5	00-041-1426
2	V_2O_5-0.5H_2O	5	00-040-1297
3	β-V_2O_5 monoclinic	5	04-014-4662
4	V_2O_5 tetragonal	5	00-045-1074
5	$H_{0.39}V_2O_5$	4.8	00-038-0009
6	$H_{1.43}V_2O_5$	4.28	00-040-1114
7	$(NH_4)_{0.38}V_2O_5$	4.62	00-027-1019

In Figure 41, the crystalline form of V_2O_5, shown in green, does not match all peaks, notably missing at 50.6°. Shown in black are other forms of V_2O_5 of valence 5 as listed in the legend; again, not all peaks are represented. Shown in blue are reduced forms of V_2O_5, valence of 4.8 and 4.28 as listed in the legend. Shown in red is a phase of V_2O_5 containing the ammonium ion, NH_4^+, of reduced valence of 4.62. Even with all these versions of V_2O_5, some peaks remained still unmatched.

4.2.2.2. $H_2V_3O_8$

$H_2V_3O_8$ is also known as V_3O_7-H_2O. This compound can result from the thermal decomposition of NH_4VO_3.[56] The reference patterns for this class had strong matches with this work's data as shown in Figure 42.

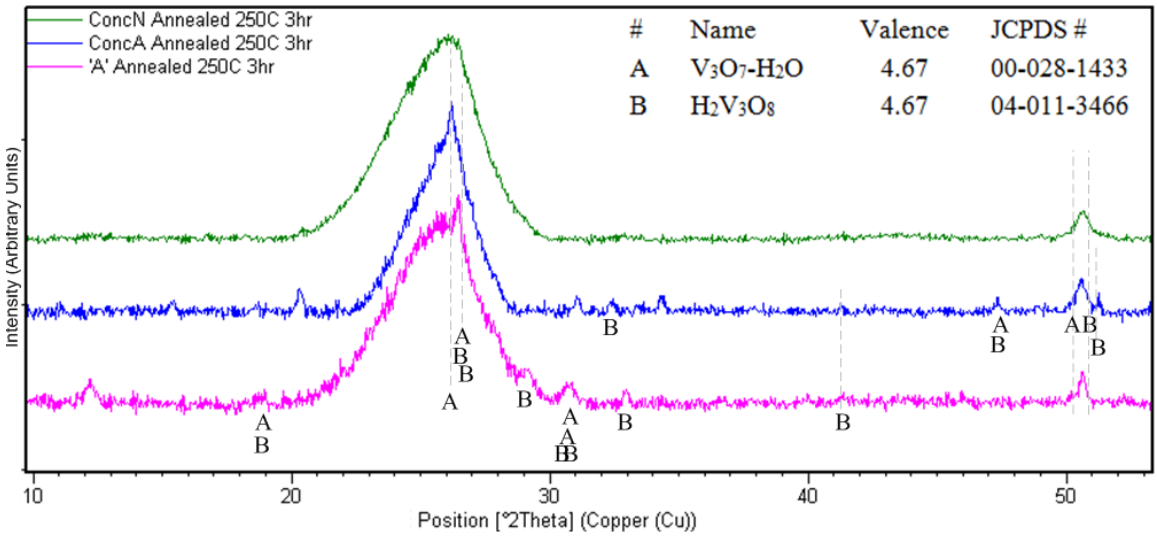

Figure 42. XRD, Annealed samples with background subtracted: Overlaid with matches to $H_2V_3O_8$ reference patterns.

From Figure 42 one can conclude that the $H_2V_3O_8$ class is present in all samples, slightly preferring ConcA based on ~26° and 51.2°, but still not a complete match:

- ConcA's peak at 26.2° is met right at peak; 'A's peak at ~26.5° is met on its right shoulder; both work for ConcN
- ConcA's 51.2° is met on shoulder
- 50.6° is met at shoulders for ConcA and ConcN, but outside shoulders for 'A'
- Some minor peaks are met in both 'A' and ConcA

4.2.2.3. Oxalates: compounds containing the oxalate ion $(C_2O_4)^{2-}$

Oxalates were a possible result of the dissolution of NH_4VO_3 with oxalic acid. [57, 58] Figure 43 shows the matches for this class of materials.

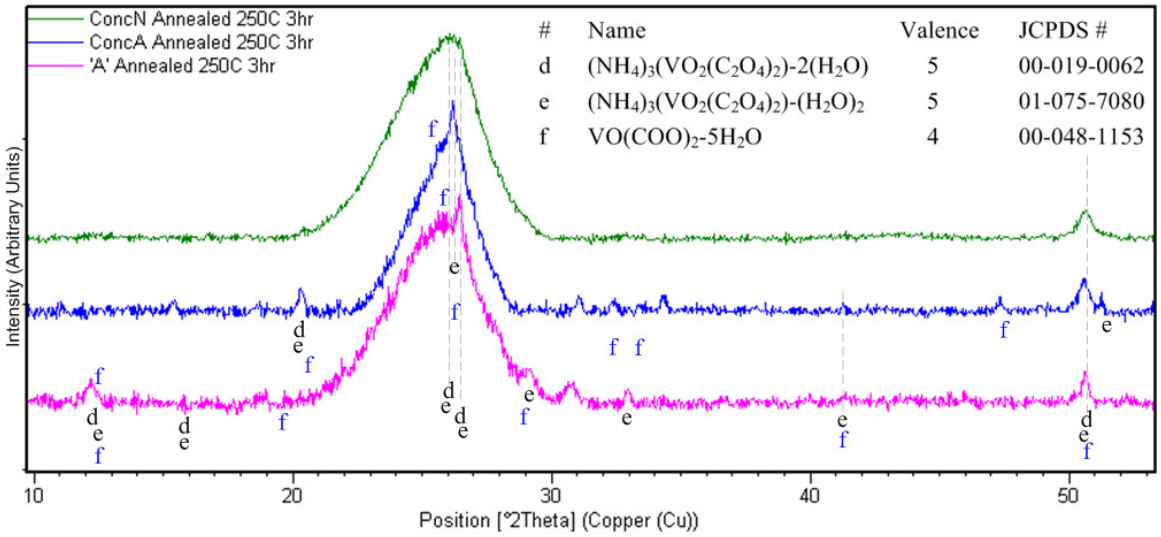

Figure 43. XRD, Annealed samples with background subtracted: Overlaid with matches to reference patterns containing the oxalate ion $(C_2O_4^{2-})$.

Oxalates of both valence 5+ and 4+ matched major and minor peaks as shown in Figure 43. Pros and cons for Vanadium ammonium oxalates comprising a part of all three patterns include:

+ Both major peaks are matched, ~26 and 50.6, on-peak
+ Some minor peaks are matched in both ConcA and 'A'

- The strongest peaks matched to ‘A’ ~12.4 and 19.7

4.2.2.4. XRD Results Summary

Conclusions from the XRD analysis are to be considered preliminary. As is apparent from the figures in this section, any given peak had several matching possibilities. The chemistry of ammonium vanadate with oxalic acid can produce many possible results. However, some trends can be stated.

- V_2O_5 appeared to be present in all samples. The crystalline form predominated in ConcA, and mixed valence forms were in all samples.
- $H_2V_3O_8$ was prominent at major peaks in all samples, and is of mixed valence. It was slightly more dominant in ConcA (considering the area around 50.6°).
- Oxalates appeared to be present in all samples, with more dominance in ’A’.
- Between these three classes, all peaks were matched.
- Due to the valence levels of the matching compounds, the overall valence of the samples appeared to be between 4.6 and 5.

Additional characterization techniques would be required to specifically identify phases from among the many possibilities presented.

4.3. Raman Analysis

Raman spectroscopy was performed by Dr. Kevin Blinn. The interpretation of the data is from him and outside the realm of this thesis author’s experience. Figure 44 shows Raman data gathered from ConcN annealed (top two lines) and ConcA annealed (bottom two lines), in two different places each. Raman measurements were taken using Argon wavelength 514.5 nm, power 5 mW and 150 second integration time.

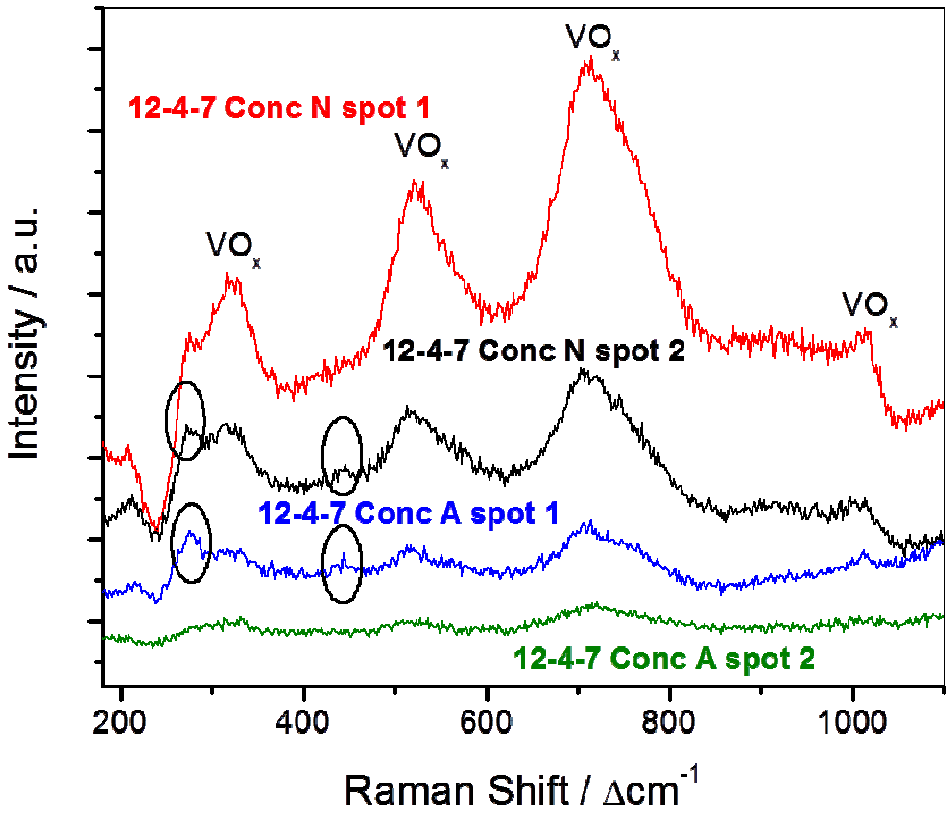

Figure 44. Raman spectra of annealed ConcN and ConcA.

The peaks labeled "VO_x" (322, 522, 713 and 1016 cm^{-1}), present in all patterns, correspond to bending and stretching modes which indicated the definite presence of some form of vanadium oxide. Possible species could have been: 522- V_2O_3 (a valence 4+ compound; although unfortunately V_2O_3 was not nearly a match in XRD); 713- polymeric; 1016- monomeric.

The circled peaks indicate variation from one place to another within the same sample. When 442 cm^{-1} was present, 275 cm^{-1} was higher; this indicated that the two were related. The variation in these peaks from one spot to another indicated that the structures were different from one spot to another. What would cause that: Mixed Oxidation (likely 4+ and 5+). This was seen on both ConcN annealed and ConcA annealed. References used in this analysis were [23], [59] and [60].

4.4. Morphology and microstructure

One of the chief goals of this study was to try to coat the CFP as well as possible; good distribution, conformal and thin. Some vanadium samples coated the carbon fibers more evenly than others, and the forms vanadium compounds took were various.

4.4.1. Bare CFP Support

Figure 45 shows bare CFP which was cleaned and annealed at 350°C for 2 hours. It was found that annealing commercial CFP at 350°C for 2 hours, or even 300°C for 30 minutes (done by others in our group), changed the CFP from hydrophobic to hydrophilic. No measurements were made but the effect was evident from observation. By comparison, an attempt at loading a piece of cleaned but un-annealed CFP never did dissipate the deposited droplets.

The surface features and texture seen in the SEM images were undoubtedly linked to the increase in hydrophilicity, and may have provided energetically favorable bonding sites. This morphology analysis will bypass the possibly-graphite white spots and focus on the features which are obviously vanadium oxides.

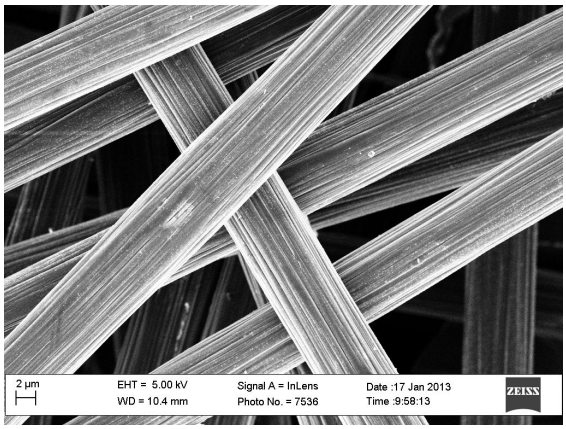

5kx

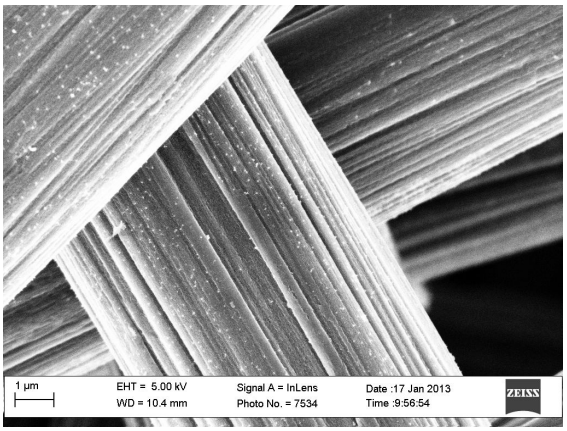

20kx

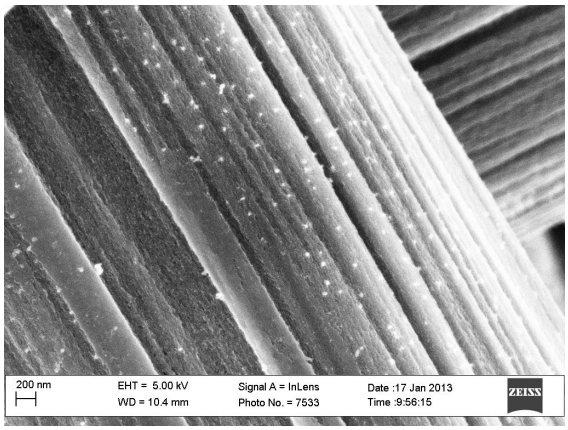

50kx

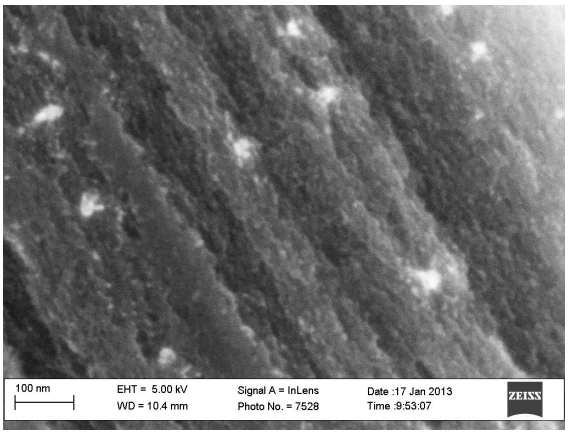

300kx

Figure 45. Cleaned carbon fiber paper (CFP) annealed at 350°C for two hours, various magnifications.

4.4.2. Vanadium Features

The amorphous nature of the un-annealed samples as indicated in the XRD patterns is also evident in the SEM images as seen in this section. It was sometimes difficult to discern the vanadium, because in the amorphous unheated state the coating was the same shade as the carbon, very smooth and well-wetting. After annealing at 250°C for three hours, vanadium features had formed and were easier to discern.

Loading of 2.1M-concentration samples was approximately 45 wt% unheated samples and 21% annealed; and loading of 1M-concentration samples was approximately 24 wt% unheated and 2 wt% annealed. These mass differences are evident in the SEM images, as the ~2M samples covered much more of the fibers than the ~1M samples.

Figure 46 demonstrates typical unheated features: in (a), well-wetting smooth patches and in (b), clumps with layered structure. The inset shows a close-up of the fibrous-appearing texture.

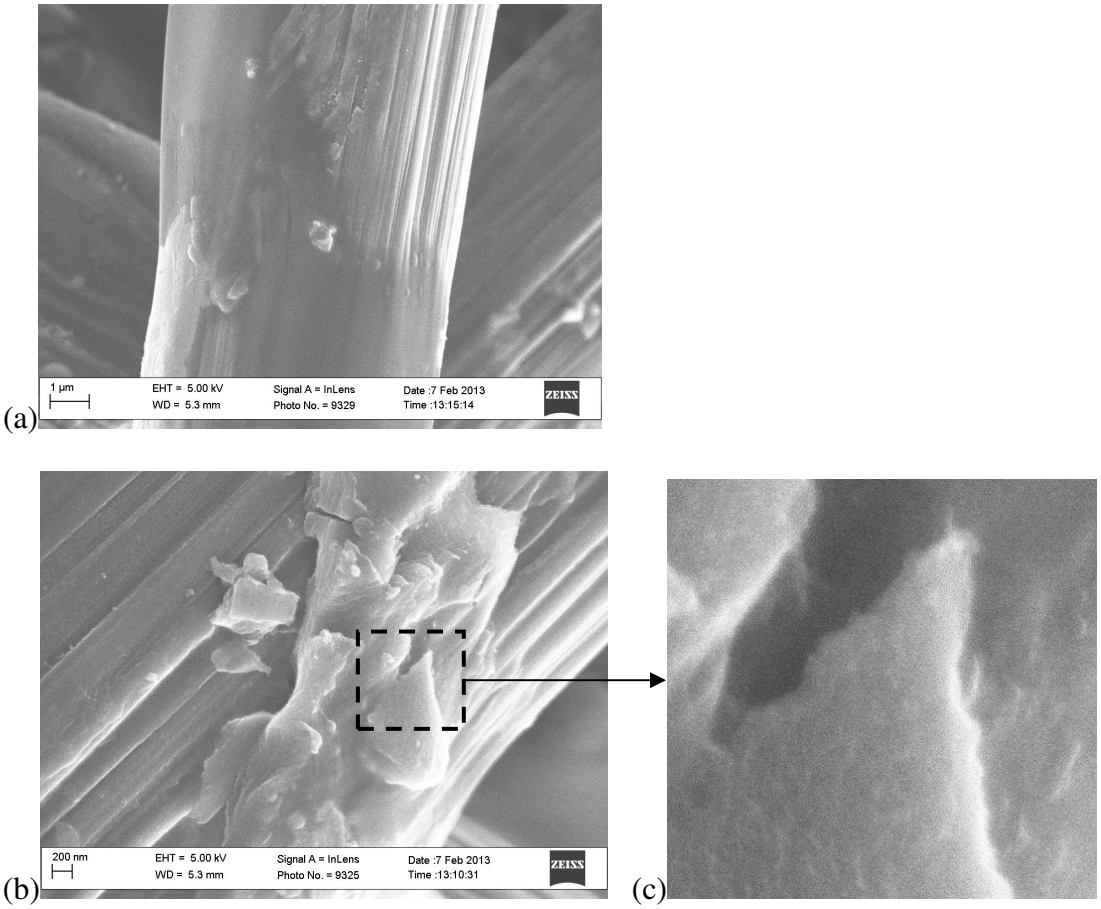

Figure 46. SEM of Unheated 2M samples. (a) 20kx, (b)50kx. (c)Inset: 200kx.

4.4.2.1. 2M concentration, Acid (ConcA)

This processing combination developed the most even and evenly thin coating. The loading did not completely cover the fibers, but the VOx was flat and evenly dispersed. Figure 47 shows the distribution over the CFP of ConcA (annealed 250°C 3hr); it is relatively even and any clumps are small. Figure 49 shows unheated ConcA; at right in the right image a patch of VOx can be discerned. In the bottom row, annealed ConcA images show a wide distribution of small nanobelts coating the resinous portions and seeming to prefer the valleys in the CFP. Figure 50 provides close-up views of the nanobelts. The estimated nanobelt size was up to 200nm long x 50nm wide.

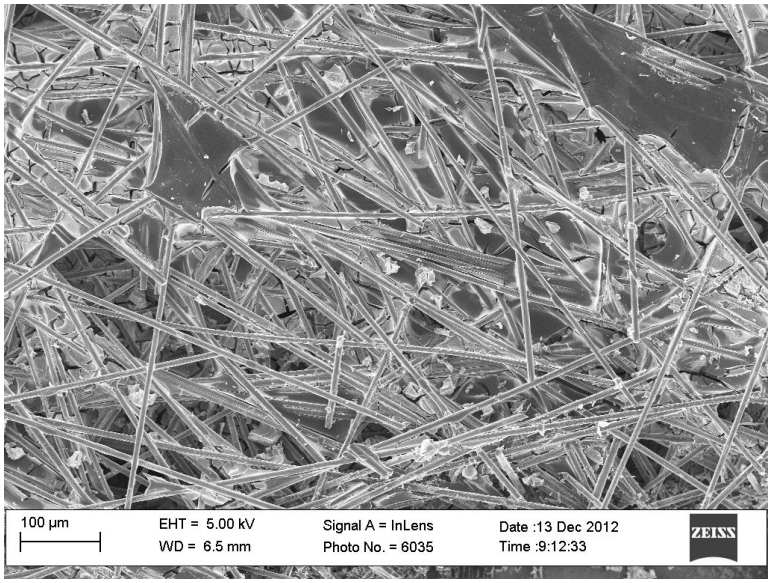

Figure 47. ConcA annealed 250°C 3hr, magnification 300x.

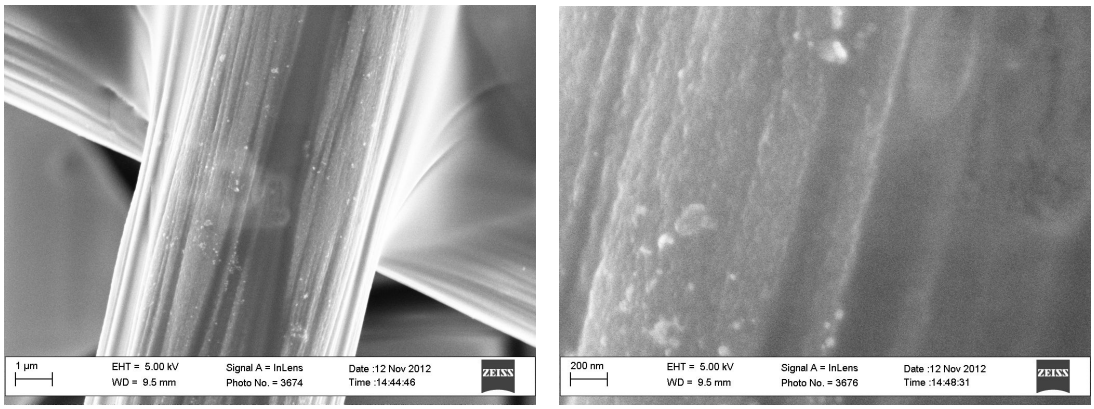

ConcA unheated 20kx ConcA unheated 100kx

Figure 48. ConcA (2.1M, acid; not neutralized) Unheated, (left) 20kx and (right) 100kx.

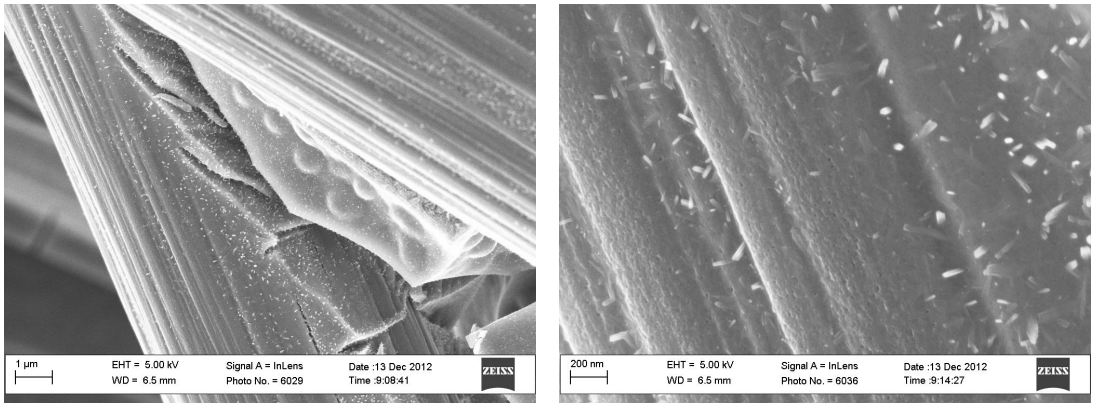

ConcA 250C3h 20kx ConcA 250C3h 100kx

Figure 49. ConcA annealed at 250°C for 3 hr; magnification (left) 20kx, (right) 100kx.

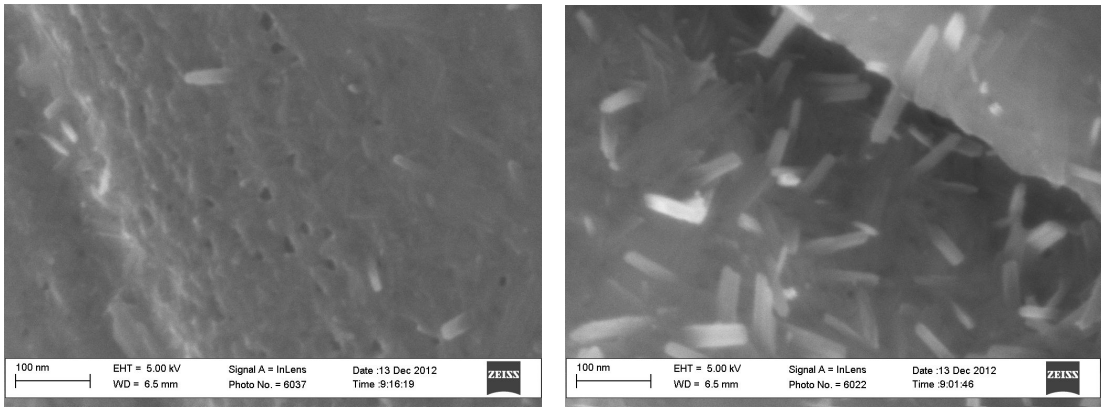

Figure 50. ConcA close-up of nanobelts, magnification 400kx.

4.4.2.2. 2M concentration, slightly Neutralized (ConcN)

The difference between ConcA and ConcN was that ConcN was partly neutralized with a half-amount of NH_4OH (half, that is, relative to V). Figure 51 shows SEM images of ConcN unheated, and Figure 52 shows SEM images of annealed samples. In the annealed samples the amorphous coating became hierarchically porous. The thinner patches appeared to have short winding fibers, and in the thicker areas, the coating changed into volumes with both macropores and nanopores. The porous zones were still well-wetted to the fibers. The estimated diameter of the macropores was 400-600nm, and the estimated diameter of the micropores was about 30nm. Figure 53 shows close-ups of the features.

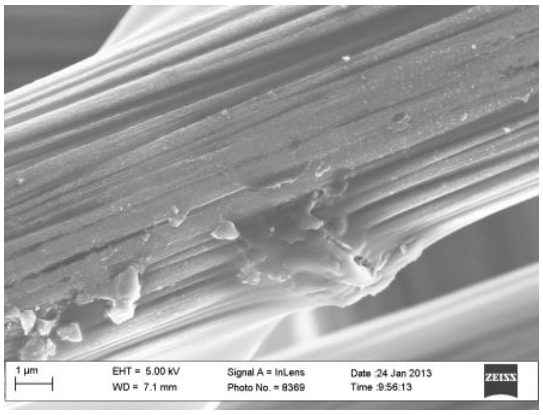

ConcN unheated 20kx

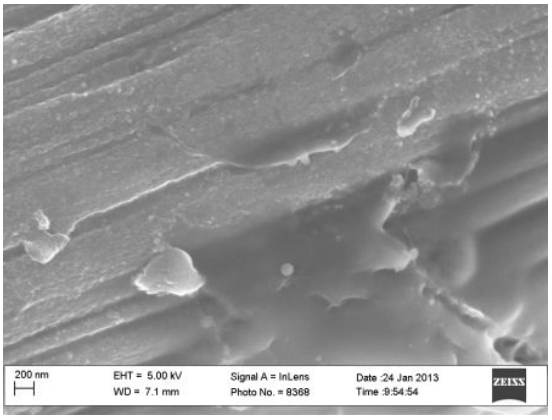

ConcN unheated 50kx

Figure 51. ConcN: 2M, partly neutralized. Unheated, magnification 20kx and 50kx.

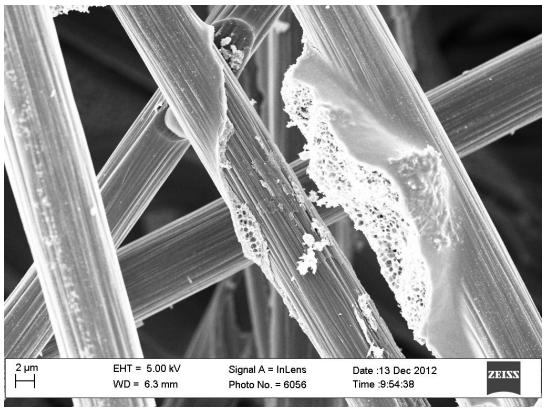

ConcN 250C3h 5kx

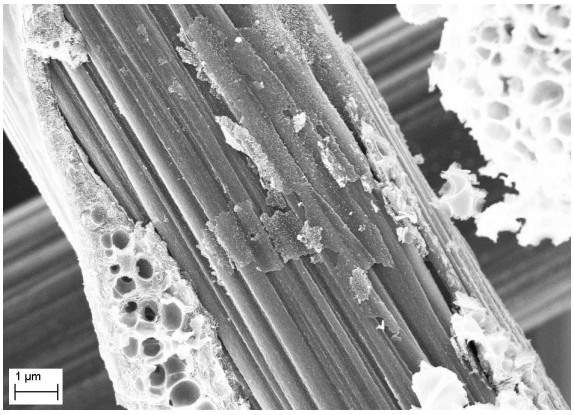

ConcN 250C3h 50kx

Figure 52. ConcN (2M, partly neutralized). Annealed 250°C 3hr, 5kx and 50kx.

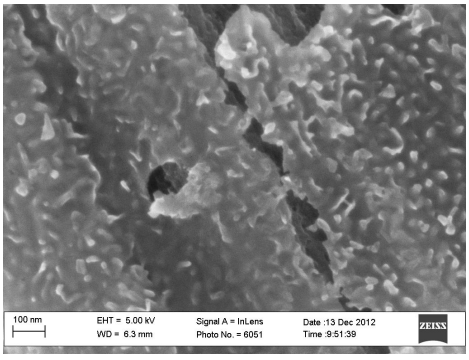

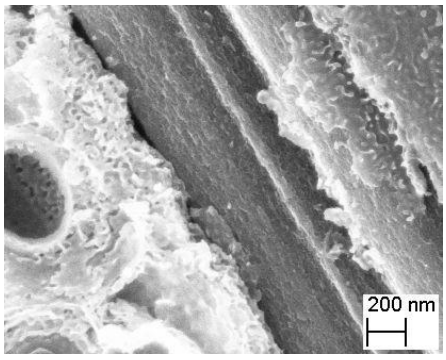

Figure 53. Detail of ConcN annealed. Left, 200kx; right, detail of 50kx in Figure 52.

4.4.2.3. 1M Concentration

On the lower concentration unheated samples, it was sometimes difficult to find the vanadium, because as well as being the same shade as the carbon, very smooth and well-wetting, it was also scarce. Nonetheless, mass difference gave assurance that vanadium coating was present.

For purpose of comparison against the better performers, the morphology of half-concentration 'A' annealed ([V]=1M, not neutralized) is shown in Figure 54. The features were highly localized, and clumped and nanocrystalline in appearance with scant

coverage of the carbon fiber. The estimated crystallite size was approximately 50nm x 100nm.

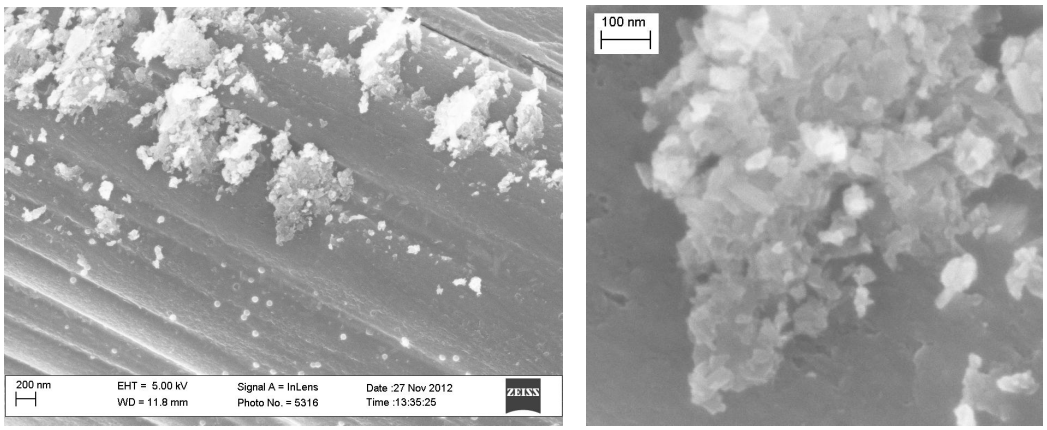

Figure 54. SEM of 'A' 250C 3hr, [V]=1M: (left) magnification 50kx, (right) 200kx.

4.4.2.4. Carbon before and after annealing loaded samples

Figure 55 shows a typical prepared bare carbon at left, cleaned and annealed at 350°C for 2 hours; at right, following annealing (shown: ConcN annealed). No visible change to the carbon surface was evident from the secondary annealing.

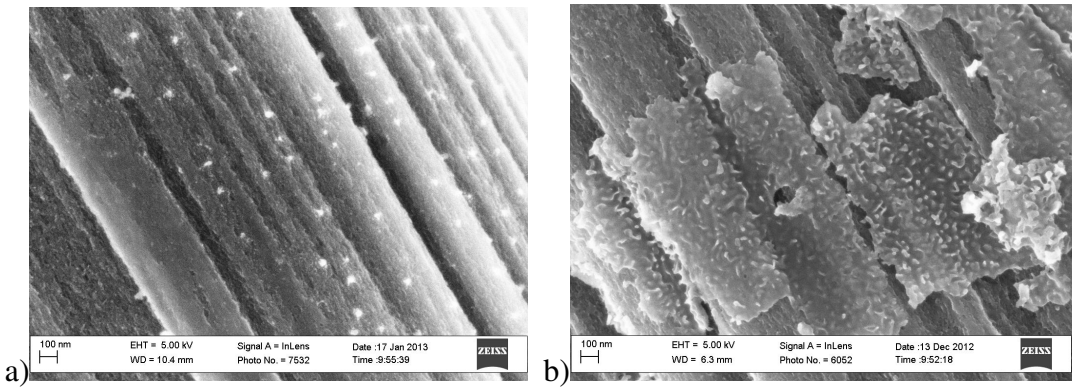

Figure 55. a) Bare carbon annealed 350°C 2hr; b) ConcN annealed 250°C 3hr, with exposed carbon. Scale bars 100nm.

4.4.2.5. Summary of morphology results

In summary, the morphologies obtained were:

- ConcA: widely dispersed thin well-wetted patches which formed closely coating nanobelts upon annealing.
- ConcN: still well dispersed over the CFP, but more clumped amorphous patches; the thicker areas annealed into a macro- and micro-porous gel, and the thinner portions annealed into the appearance of twisting fibers (i.e., a xerogel) in a thin bed of amorphous material. The porous coating appeared to maintain a good connection to the fiber.
- A: amorphous flat pads of vanadium oxide annealed into localized assemblies of nanocrystals.

4.5. Summary of results

Amount of loading and coverage:

- Incipient wetness impregnation of CFP, given pore volume of 77%, loaded the 2.1M samples to ~45 wt% unheated and ~21wt% annealed at 250°C for 3 hours; and loaded the 1M samples to ~24 wt% unheated and ~2 wt% annealed at 250°C for 3 hours.
- The lower concentration (1M) had too scarce coating on the CFP; most of the surface was bare upon annealing.
- The higher concentration (~2M) covered most of the fibers but not completely and there was some minor clumping, more so in ConcN than in ConcA.

Electrochemical performance:

- Cyclic voltammograms were nearly symmetrical and had no redox peaks.

- Galvanic cycles had very little IR drop, and for ConcA showed a slight curvature characteristic of pseudocapacitance.
- The samples of concentration [V]~1M had areal capacitance slightly better than bare hydrophilic-treated carbon, approximately 0.62-0.70 F/cm^2.
- The samples of concentration [V]~2M with widespread nanofeatures had areal capacitance more than twice as high as carbon, approximately 1.0-1.2 F/cm^2.

Morphology and phase:

- All unheated samples were amorphous with no XRD peaks, and well-wetted patches and clumps on the fibers.
- All annealed samples in the incipient wetness method had an XRD peak characteristic of V_3O_7-H_2O, a mixed-valence phase, as well as peaks from other mixed-valence phases and valence 5+ phases of V_2O_5 and vanadium oxalates. The overall valence was, by the phases, possibly 4.6- 5.
- The more concentrated samples formed electrochemically favorable nanofeatures: nanobelts (pH~1.5) and porous xerogel (pH~2.0).
- Slightly more neutral samples developed very little crystallinity according to XRD.
- 1M low-pH samples coated the fibers sparsely, and the acidic samples formed patches of nanoparticles of crystalline appearance.

CHAPTER 5: DISCUSSION

Herein are brought together elements from all three characterization methods – electrochemical, XRD and SEM – to make connections between processing, morphology and performance.

5.1. Processing

5.1.1. Solution Preparation

By warming the solution but keeping the water bath below 100°C, solids could dissolve but NH_4^+ could remain in solution. The presence of NH_4^+-containing compounds in the XRD matches (to be highlighted in Figure 56) provides evidence of NH_4^+-rich solutions.

5.1.2. High Concentration

High concentrations of vanadium in aqueous solution have received little study, so hopefully this work added new information to the body of knowledge. The highly concentrated samples coated most of the fibers, and maintained a relatively flat, close profile to the carbon even after annealing. The annealed high-concentration oxides in this study had higher areal capacitance and specific capacitance than those of half the concentration, as illustrated in Figure 33.

5.1.3. Incipient Wetness Impregnation

The Incipient Wetness (IW) impregnation technique was described in section 2.5. It proved to be successful at distributing a known amount of vanadium evenly over and throughout the CFP. Furthermore the method is quick and inexpensive, cost-effective

because it uses less equipment (no hydrothermal treatment or ion exchange resin) and does not require aging (time is money) or supercritical drying (more steps, controlled environments).

Consistently across the literature, combining carbon with vanadium oxides improves electrochemical performance over vanadium oxides alone. One example is [30] but there are many. The incipient wetness method used in this study fabricated binder-free electrodes onto inexpensive CFP providing a continuous conductive support.

5.1.4. Carbon Annealing

The pre-treatment of the carbon fiber paper was essential to rapid, even dispersal of solution upon loading. The CFP thermal treatment done as described in sections 3.2.2 and 4.4.1 was analogous to thermal functionalization done for longer times (10 hours) as described in section 2.4.[45] In both cases, at 350°C the CFP became markedly more hydrophilic and did not combust.

The benefits of annealed CFP were threefold:

First, the dynamics of solution spreading were improved by the CFP becoming hydrophilic.

Second, surface area increased due to the more highly textured surface; this is always a benefit for pseudocapacitors.

Third, hazardous nitric acid was not required.

5.1.5. Intermediate temperature for annealing

As discussed in section 2.2.2.1, annealing to 250°C removed all the 'easy' water loosely bound between layers. By maintaining 250°C for three hours, it was predicted that the water loss would be irreversible. By limiting the temperature to not higher than

this point, it was predicted that V_2O_5 would not fully crystallize. The XRD patterns support both these hypotheses; small broad peaks showed that little crystallinity was developed, and the patterns did not match any of the more-hydrated forms of V_2O_5.

As shown on Figure 35 in section 4.1.3, in this study annealed samples had higher capacitance than unheated samples. This is undoubtedly due to the nanofeatures (and possibly phases) formed. It is possible that moderate annealing temperatures allowed beneficial microstructures to form and not break down. In reference [44] it was shown that annealing a xerogel at 260°C broke down the fibers; see Figure 21 in section 2.3.4.

From the literature, sections 2.3.2 and 2.3.3 describe work by others in which specific capacitance was higher for annealing at low to moderate temperatures than at higher-temperature annealing. Perhaps this study might be another case in which intermediate annealing temperatures are optimal.

5.1.6. Choice of chemicals

The choice of oxalic acid to dissolve the vanadium enabled reduced valence compounds and oxalates to form, and was preferable to using other more hazardous chemicals such as hydrazine.

The combination of NH_4VO_3 and oxalic acid is relatively common in catalyst literature but less so in pseudocapacitance literature. This study represented the opportunity to expand that knowledge base. The fortunate result was respectable areal capacitance. The ammonium-based precursor may have been instrumental in the morphology of ConcN as will be discussed in section 5.2.3.2.

Oxalic acid is commonly used to dissolve vanadium, and in excess amounts acts to reduce vanadium. The 1:2 ratio of NH_4VO_3 to oxalic acid resulted in mixed-valence

compounds. Several reduced-valence phases matched peaks in the XRD of all samples (section 4.2.2).

It is also possible that oxalic acid facilitated the bond between the coating and the carbon. In section 2.5 further details are provided to support this idea.

With NH_4VO_3 as the vanadium precursor, shifting pH to more neutral with ammonium hydroxide added no new elements to the solution. Adding a half-amount of ammonium hydroxide per vanadium shifted the pH from 1.5 to 2, and shifted the morphology from nanobelts to porous xerogel.

5.2. Phase, Morphology and Performance

5.2.1. XRD Results Analysis

XRD evaluation in this study can only be considered an approximation. XRD references for intermediate levels of annealing are scarce, especially for compounds besides V_2O_5 or VO_2; also, most peaks had multiple possible matching phases. Nonetheless, an attempt will be made to discern trends with the phases shown to match in section 4.2.2. In the figures to follow, V_2O_5 are squares, $H_2V_3O_8$ are triangles, and Oxalates are circles.

To further discern the presence and possible influence of reduced valence and ammonium, phases have been filtered in different ways and displayed in the next several figures.

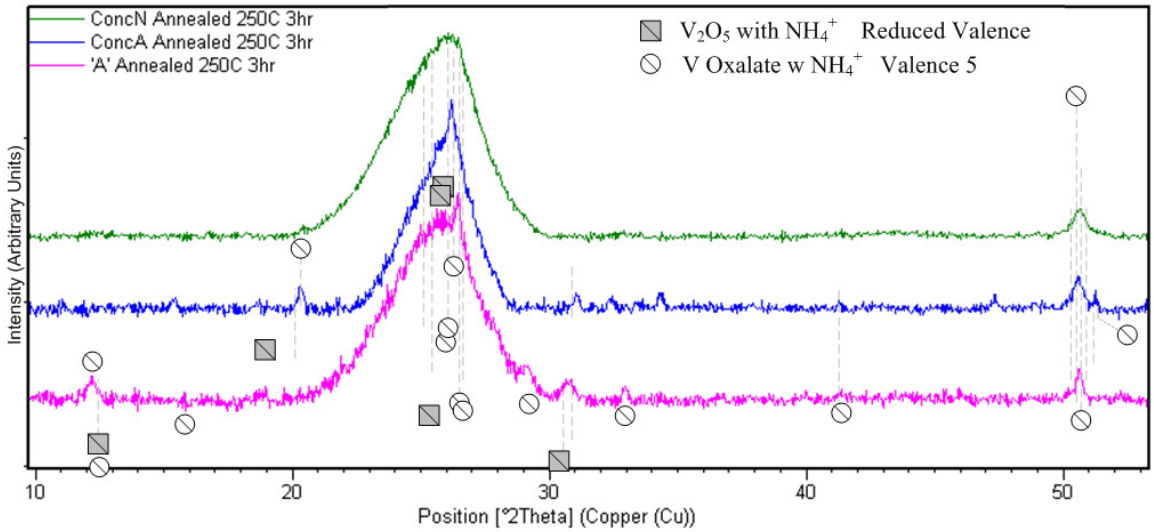

Figure 56. XRD, annealed samples with background subtracted, matches to reference patterns: only **compounds containing NH_4^+**.

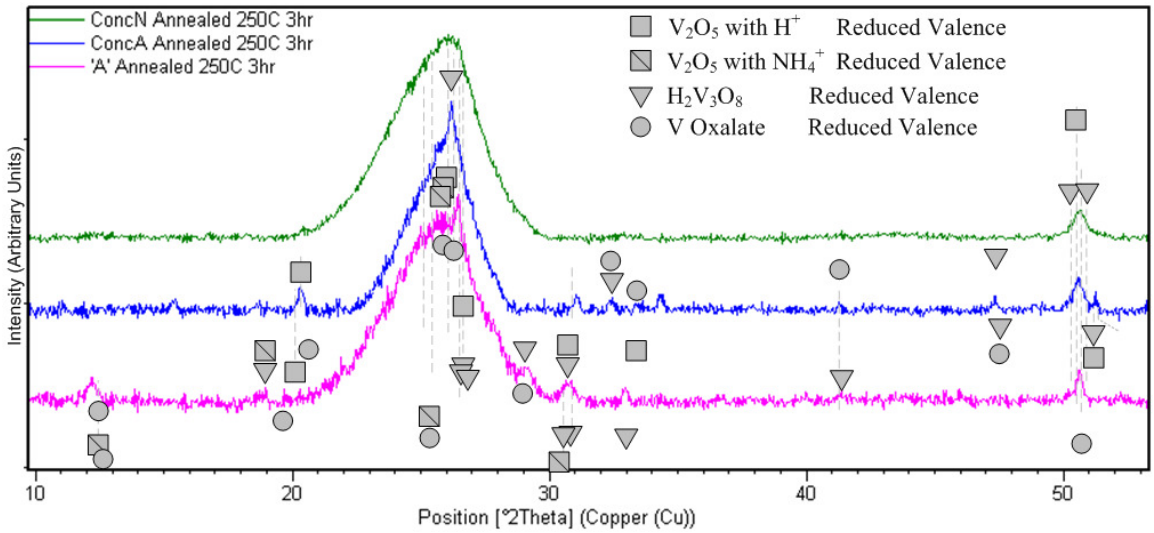

Figure 57. XRD, annealed samples with background subtracted, matches to reference patterns: only **reduced valences**.

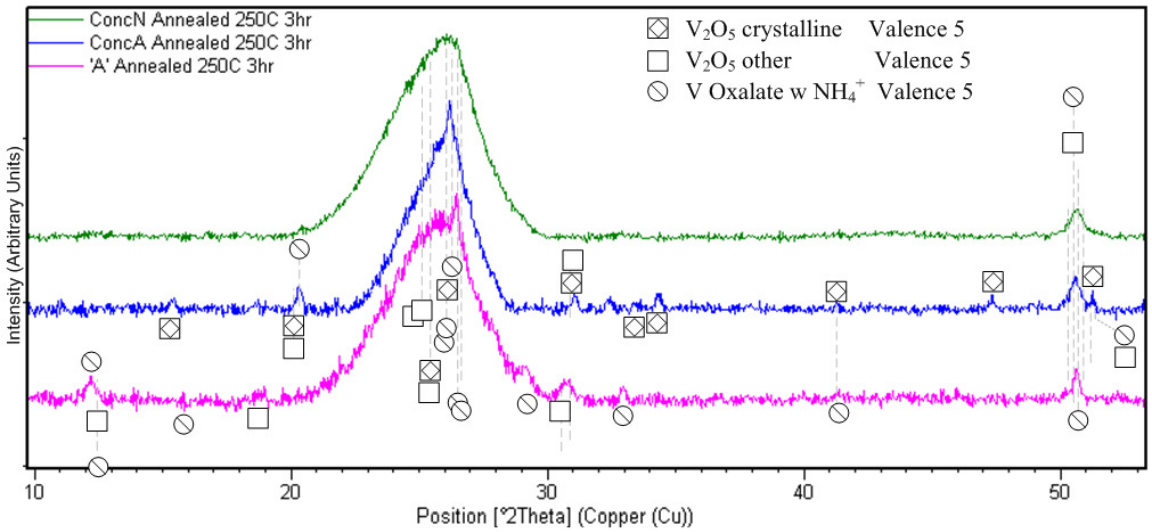

Figure 58. XRD, annealed samples with background subtracted, matches to reference patterns: only compounds of **valence 5+**.

In an effort to simplify phase analysis, a comparison was made of only the strongest peaks from the references. This is shown in the next figure. From this figure it is clear that reduced-valence phases had a strong influence in all patterns.

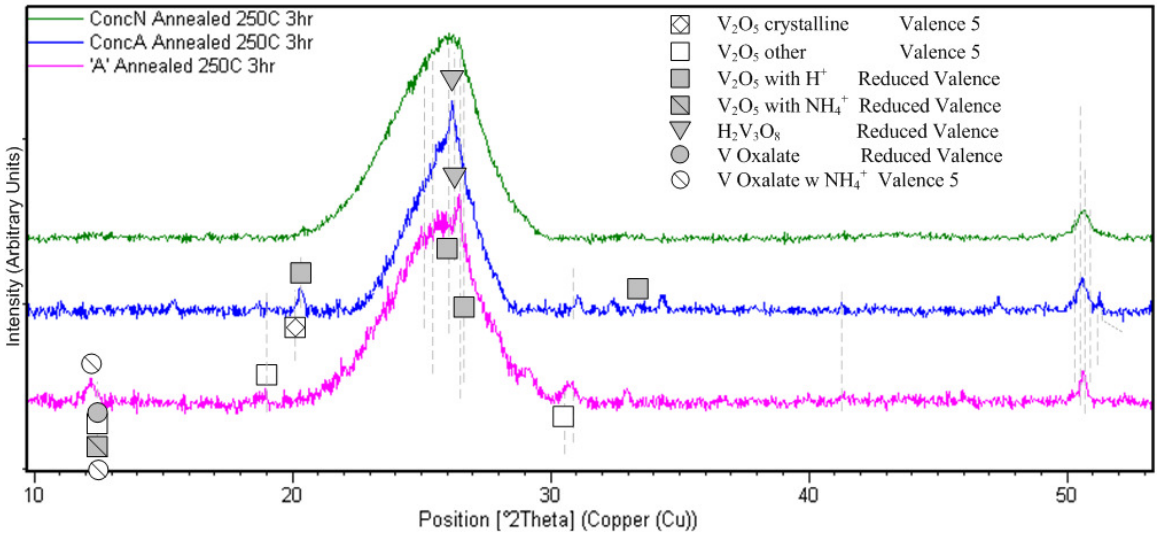

Figure 59. XRD, annealed samples with background subtracted, matches to reference patterns: **major peaks of reference patterns** matched

The peak at 50.6° was not a major peak in the references but was obviously important in the data. A comparison was made among the reference patterns for the strength of match around the peak at 50.6°. In the reference pattern for V_3O_7-H_2O, the peak for 50.6° is markedly stronger than in the other classes. The next strongest 50.6° candidate was the oxalates, then the ammonium-V_2O_5, and finally in the remaining V_2O_5, 50.6° were all quite small. A similar comparison could not be distinguished for the peaks around 26°. This analysis suggests a higher probability that the $H_2V_3O_8$ phase was present in all samples.

Finally all the phase categories are shown together in the next figure.

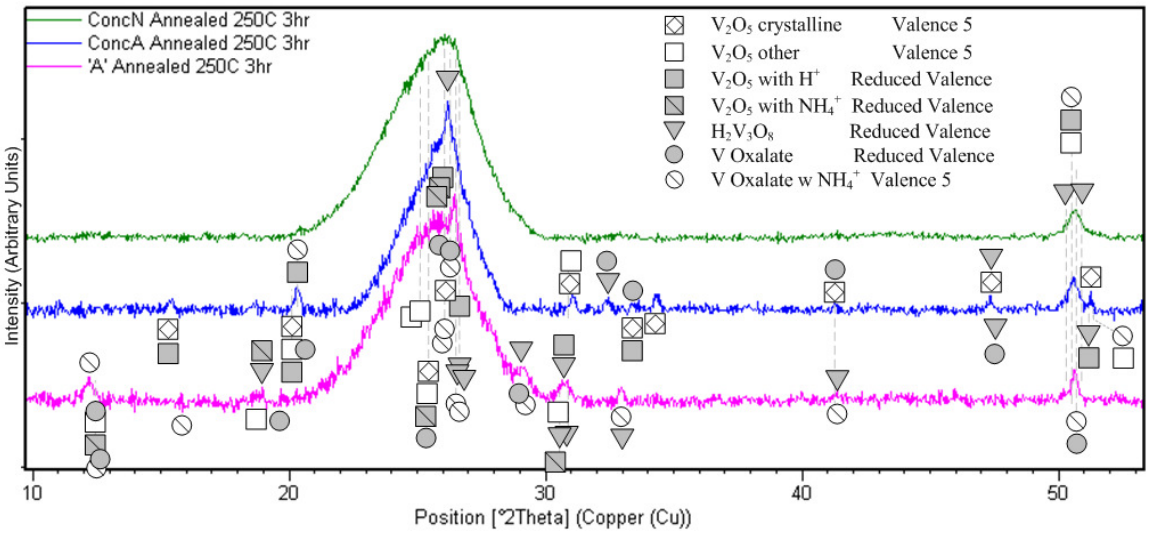

Figure 60. XRD, annealed samples with background subtracted, matches to reference patterns: **all phases together**.

Some tentative conclusions can be drawn from this analysis, which would need to be confirmed with other characterization techniques:

- ConcA is more strongly V_2O_5 of mixed crystallinity.
- 'A' is more strongly vanadium oxalates.
- ConcA, ConcN and 'A' all have reduced valence.

- V_2O_5 and $H_2V_3O_8$ are in all samples.

The Raman analysis from section 4.3 also concluded that both ConcA and ConcN were of mixed oxidation.

5.2.2. Phases

Phases described in this section showed similarities in XRD, and also have characteristics in common with this study.

5.2.2.1. V_2O_5

V_2O_5 is one of the more stable, commonly-researched forms of vanadium oxide (most often for lithium-ion batteries). The XRD data in this study had many close matches with V_2O_5 reference patterns, and the patterns also closely resembled those of micro- and nanosized V_2O_5 in the literature. ([42], Supplemental Information, and [22]) V_2O_5 could be a possible product of NH_4VO_3 conversion via thermal decomposition [56, 61], or a product of chemical reaction via a number of paths.

As discussed in section 2.2.2.1, V_2O_5 loses H_2O upon heating, arriving first at stable orthorhombic but non-crystalline V_2O_5-$0.5H_2O$, and above a certain temperature crystallizing to orthorhombic crystalline V_2O_5, also known as shcherbinaite. The intermediate phases are difficult to distinguish in XRD, but some studies have shown enhanced capacitance from intermediate, pre-crystalline phases formed by annealing at moderate temperatures (200°C, 250°C, and 300°C) ([18, 43]; sections 2.3.2 and 2.3.3). The XRD of this study had elements in common with the XRD of both of these studies' higher-performing samples. This study's XRD's also had strong similarity with the XRD

of the carbon tube-in-tube experiments, done with the same precursors, shown in section 2.3.1.

Morphology is often used to improve the electrochemical performance of V_2O_5. In every study found in which nano-sized features were formed, V_2O_5's electrochemical performance was improved. V_2O_5 can form many shapes including porous xerogels to aerogels, nanowires, belts, urchins, and wavy thin structures. In this study there was not time for nanowires or other long features to form, but as seen in SEM, small features formed; nanobelts of approximate dimensions 50nm x 200nm, and micropores of approximate diameter 30nm.

The electrochemical performance of V_2O_5 has also been improved by the presence of carbon in many ways, as indicated in section 2.3. [18, 42]

5.2.2.2. $H_2V_3O_8$ /V_3O_7-H_2O

These phases, as described in section 2.2.3.4, are mixed-valence compounds (valence 4.67) demonstrated to have pseudocapacitive performance (examples listed in Table 3), and are known to form xerogels, nanowires and nanobelts. They could be expected by way of V_2O_5 and oxalic acid ([62], [63] and [26]) or by thermal decomposition and subsequent reduction from NH_4VO_3.[56]

$H_2V_3O_8$ phases (to use the more current name) matched in all XRD patterns at both major and some minor peaks, with seemingly a slight preference for ConcA over 'A'. The benefit of $H_2V_3O_8$'s presence in this study is mixed valence and pseudocapacitance enhanced by its influence on nanostructure.

5.2.2.3. Oxalates and benefit of nanoscale

Oxalates can result from mixing NH_4VO_2 and oxalic acid; for example, in [12] the result is $(NH_4)_2[VO(C_2O_4)_2]$, with valence 4+ and a deep blue color. Other possible oxalate products are discussed in [57] and [58].

An untested hypothesis is that perhaps the oxalates were used up in ConcA and ConcN in the process of bonding to the CFP. This Incipient Wetness bonding step is described in section 2.5. 'A' had less material to bond, and relatively more water in solution, so its chemical dynamics were different.

Sometimes oxalates are used to transform normal V_2O_5 into nano-sized V_2O_5; one example is [22]. In that work, nanostructured V_2O_5 formed by way of reaction product vanadium oxalate (VOC_2O_4), a compound containing several peak-matches to this study. Vanadium oxalates were likely intermediate compounds in this study, and the nanocrystals seen in 'A' bear some resemblance to nanoparticles formed in [22].

5.2.3. Morphology Effects from Processing

5.2.3.1. Effect of annealing temperature

In section 2.3.3 the effect of annealing temperature on V_2O_5 thin films was examined (Figure 20). Important trends were: specific capacitance higher for films annealed at 250°C and 300°C than those annealed at higher temperatures; pores forming between 250°C and 300°C, then disappearing; and the change from basically flat at 250°C to islands by 400°C. The precursors and substrate were different, but possibly some of the trends could apply.

Relating these trends to this study, one could wonder whether limiting annealing to 250°C may have kept the coating smoother and more evenly spread out than if

annealing had been done at higher temperatures. Consider, for instance, the even distribution of nanobelts in ConcA (Figure 49) and xerogel in ConcN (Figure 52). One could also wonder if higher annealing would break down the pores formed on ConcN. Further study would be needed to answer these questions.

5.2.3.2. Xerogels, in the presence of Nitrogen while heating

Figure 21 shows oxynitrides resulting from annealing xerogels under nitrogen. This process allowed the gels to keep their fibrous nature longer than they normally would have under annealing temperatures used. The morphology of the features strongly resembles the fibers in the xerogel of ConcN.

The XRD patterns in this study had many matches to compounds containing NH_4^+ in all samples (see Figure 56). It is possible that this residual NH_4^+ provided a similar environment to keep nanowires in ConcN from breaking down under annealing.

5.2.3.3. Flatness of coating and conformality

The coating formed by the incipient wetness impregnation method was well-wetting to the fibers, forming broad smooth areas. This happened when pH was ~2 or less. Above this pH, the unheated coating exhibited large clumps.

Vanadium oxides applied as a sol will always experience shrinkage unless they undergo supercritical drying, due simply to the large volume formerly occupied by H_2O. By one estimate the shrinkage loss after a sol-gel deposition was 50%. [64] Subsequent annealing removes more water and shrinks it further.

Still, ConcN and ConcA managed to retain coverage over most of the fiber through drying and annealing. In ConcN, small areas of VOx did pull aside as the porous features developed, but still left the fibers mostly covered; both the thickly and thinly

coated areas also remained generally flat. The pore-formed areas maintained a close connection with the CFP whereas the thin xerogel-like mats pulled partly away from the surface. In ConcA, the developed nanobelts maintained a close connection to the fiber; any volume lost was condensed into the nanobelts themselves. In both cases, the good hold maintained on the CFP could be attributed to its functionalization. In the case of reduced concentration, too little VOx remained through drying and annealing, and evidently the drive to aggregate was stronger than the drive to stay in place and grow nanofeatures.VOx subunits do tend to join at edges and corners to reduce energy.

5.2.3.4. Xerogels

Xerogels, described in section 2.2.3.1, can appear in SEM as amorphous clumps in which no linear features visibly appear. Many phases of vanadium form xerogels, with a fibrous nature only apparent at very high magnifications (Figure 14). Some of the clumps found on some of the unheated CFP fibers in this study fell into this category. As described in section 2.3.2, when researchers formed V_2O_5 xerogels incorporating activated carbon, specific capacity was enhanced. [18] The xerogel of that work bears in common with this study a subdued level of annealing, a peak just above 50° in the XRD pattern, morphology of some unannealed samples, and carbon benefit.

5.2.4. Mixed Valence

The oxidation level of the vanadium compound has a large effect on its pseudocapacitance. (Recall that pseudocapacitance involves an exchange of charge into the top few nm of the electrode.) Mixed valence is important to pseudocapacitors, because reduction/oxidation reactions take place between V(II)/V(III), V(III)/V(IV), and

V(IV)/V(V) valence pairs. Using a 1:2 ratio of ammonium vanadate: oxalic acid assured that the vanadium would be reduced at least partly.

The oxidation level is sometimes indicated by the color of solution; for example, in a vanadium flow battery, one observes V^{5+} yellow, V^{4+} blue, V^{3+} green, V^{2+} violet; but one cannot always identify valence level by color alone. Vanadium compounds can be orange (as in V^{5+} V_2O_5), green (mixed V^{4+}/V^{5+}), black (V^{4+}), blue, brown, pink, yellow, or red. The solutions described in this study were dark blue tinged with purple, and when ammonium hydroxide was added to neutralize they shifted to dark green. These colors are stated as a point of interest.

The XRD patterns of this study have many matches to mixed-valence phases, both from reference patterns and the literature, and no clear match to any one single phase. This is a clear indication of mixed valence vanadium oxides.

The mixed-valence compounds described in section 5.2.2.2 ($H_2V_3O_8$) have been shown to be intermediates or products in VOx fabrication from solution. Their pictured morphologies are similar to forms found in this study; nanobelts, nanocrystalline particles, and xerogels made from nanowires. Likewise, reduced-valence oxalates (VOC_2O_4) such as described in section 5.2.2.3 have been shown to be intermediate compounds in nanosized VOx fabrication. All these compounds matched peaks in this study's XRD, indicating mixed valence.

In short, all indications – chemical amounts, XRD patterns, colors, specific capacitance – point to mixed-valence results. The precise phases could not be definitively identified, but this is the case in many vanadium oxide studies.

5.2.5. Degree of Crystallinity

XRD was examined for signs of crystallinity. The peaks that began to develop upon annealing were short and broad; this could indicate that crystallinity was not strongly developed, or that the crystallite size was very small. (Grain size is inversely related to peak width through the Debye-Scherrer equation. Note: peak dimensions and grain size metrics were not analyzed in this study.)

In Figure 41 which features the XRD reference patterns of V_2O_5, the crystalline form of V_2O_5 is shown in green; it does not match all peaks (notably missing at 50.6°). This pattern was not expected to match completely, as the annealing temperature was not high enough to fully crystallize the coating into V_2O_5 (Section 2.2.2.1). If future work using additional characterization techniques were to show that shcherbinaite was in fact formed, this study would represent a lower-temperature method of forming that compound.

Samples with highest crystallinity were not necessarily the highest in areal capacitance. ConcA was more crystallized than ConcN but the two had approximately equal areal capacitance. ConcA was slightly more crystallized than 'A' (judging for the moment by the sharpness of XRD peaks rather than matched phases) but had far superior electrochemical performance to 'A'.

Annealing to full crystallinity does not optimize pseudocapacitance (as discussed in section 5.1.5); but on the other hand, in this study some amount of annealing was required for good performance. In this study an intermediate path was taken; annealing was kept below levels at which fully crystalline phases would have formed.

Unheated samples were always lower in specific capacitance than their annealed counterparts, and were always amorphous with no nanofeatures. In the case in which the annealed sample was also amorphous (ConcN), the porous gel nanostructure provided high specific capacitance without crystallinity. In the cases in which the annealed samples were partly crystalline (ConcA and 'A'), primarily coverage and morphology made the difference between average and good performers.

5.2.6. Theory for Nanobelts in ConcA

Some of the phases shown to match with ConcA's XRD patterns have been demonstrated to form layered structures and nanobelts as discussed in section 2.2.2; V_2O_5 (Figure 16) and V_3O_7 (Figure 15). ConcA also has a markedly more pronounced effect of crystalline V_2O_5 as seen all over the pattern.

Under normal circumstances, higher heat is required to reach crystalline V_2O_5, e.g. $\geq 350°C$. Possibly thermal reduction of oxalates accelerated this process as mentioned in section 2.2.3.5.[22] An alternate explanation could be that the structure of an as yet unspecified complex phase was very similar to that of crystalline V_2O_5; i.e., orthorhombic with approximately the same dimensions.

In hydrothermal treatment, VOx has a long time to grow nanowires and nanoribbons; in this study, nanofeatures were formed during the 3-hour annealing process; therefore, they are small and short.

5.2.7. Theory for Porous Xerogel

The porous xerogel of ConcN was marked by three characteristics: amorphous phase, nanofibers in smooth gel, and pores where the coating was thicker.

The amorphous nature of ConcN was undoubtedly influenced by its pH and valence level, as all vanadium oxides are. When considering the phase diagrams in Figure 6, at high concentrations of aqueous solution at pH=2 and valence 5, one has solid V_2O_5; while at pH=2 and valence 4, one has an aqueous species. Phase diagrams were not located for V-O-H-N systems, but one can extrapolate that in a mixed valence solution, the solution might be a mixed phase.

It is the theory of the author of this thesis that ribbon and porous gel formation in ConcN was influenced by the presence of residual NH_4^+. All of the XRD patterns had matches in XRD to compounds containing NH_4^+ (Figure 56); this indicates a strong likelihood that some NH_4^+ remained in all solutions due to the solution preparation process. The neutralized mixtures had additional NH_4OH, increasing the NH_4^+ presence.

Evidence for residual NH_4^+'s role in ConcN morphology includes:

- Flexible ribbonlike features in the more thinly-coated patches had a visible appearance similar to a xerogel and to the oxynitride xerogel shown in Figure 21c.
- Precursor NH_4VO_3's structure is that of a one-dimensional string (Figure 8a).

A possible explanation for pore formation could be that NH_4^+ became gaseous upon annealing, forming pores in the thicker regions of the coating. Another, or additional, explanation could be intermediate-temperature annealing as discussed in sections 2.3.3 and 5.2.3.1. Pores in a thin V_2O_5 film were formed at 300°C and were gone by 350°C.

5.2.8. Electrochemical Perspectives

Based on the specific capacitance results presented in Figure 34, some speculation can be given with regards to the effect of the morphology on performance. Although layered vanadium oxides can intercalate sodium from aqueous electrolyte [4], if intercalation were a large effect (especially bulk intercalation as in Li-ion batteries), the capacitance would have been markedly higher for the slower scans, as intercalation is a slower process than the other pseudocapacitance mechanisms. Instead, the capacitance was roughly constant for ConcN, and reached a maximum at 5 mA/cm^2-s for ConcA. Besides layers for intercalation, morphology can offer other benefits for electrochemical performance:

- Adsorption and all other pseudocapacitance mechanisms benefit from increased surface area.
- Nanopores shrink the diffusion distance for any interaction with ions from electrolyte, thereby speeding any process depending on diffusion.

Hierarchically porous, amorphous ConcN provided ample surface area for all pseudocapacitive processes. ConcA also provided much surface area via its more-crystalline nanobelt surfaces, with layers instead of micropores housing short diffusion distances. It is seems that ConcA's geometry provided an improved structural environment for reaction sequences proceeding at certain galvanic cycling rates. However, it was not the intention in this study to explore intercalation or to determine the active pseudocapacitive mechanism; to do so, three-electrode testing would be required. Instead, this study was conducted to narrow the field to those contenders worthy of more in-depth study.

CHAPTER 6: CONCLUSIONS

6.1. Conclusions

The incipient wetness impregnation technique was successfully used to coat hydrophilic carbon fiber paper (CFP) with vanadium oxides in a manner which was well-wetted and well-distributed throughout the CFP. Fabrication conditions were optimized to produce electrodes with respectable electrochemical performance.

The methods used were cost-effective and environmentally minimally impactful. Commercial CFP (cheaper than carbon nanotubes) provided a continuous current-carrying network without the use of binder, and functionalizing it thermally avoided the use of hazardous chemicals. By using the incipient wetness method, all vanadium ended up on the electrode; there was no waste solution left over as with hydrothermal or other methods. Special environments and long treatment times were not required.

The electrochemical performance was evaluated in two-electrode cells for quick screening and comparison, and it was found that areal capacitance was higher for samples annealed 250°C for 3 hours in air, and highest for samples from high concentration solutions (2.1M) of pH <=2 which developed broad distributions of nanofeatures during annealing.

Oxalic acid in a 1:2 vanadium precursor:oxalic acid ratio assisted in dissolving the vanadium and also reduced its valence for enhanced pseudocapacitance, and may have had a role in bonding to the CFP. NH_4^+ in solution may have contributed to beneficial nanofeatures such as xerogel and porous gel upon annealing. Annealing to the moderate temperature of 250°C for three hours removed most of the H_2O from vanadium oxides

yet kept the material below the level of fully crystallizing to V_2O_5 shcherbinaite. This temperature and time most importantly allowed beneficial nanofeatures to develop.

The relatively even, close-forming coating afforded by the incipient wetness procedure as employed in this study enabled nanofeatures to develop in relatively conformal patches rather than freestanding clumps.

In ConcA, mixed-valence VOx nanobelts provided areal capacitance of 1.0-1.2 F/cm^2 or specific capacitance of approximately 380-450 F/g.

In ConcN, a solution neutralized slightly with half-amount ammonium hydroxide resulted in mixed-valence porous VOx xerogel with capacitance of approximately 1.1 F/cm^2 or 450 F/g.

Even A, with its scant coverage due to lower solution concentration, offered an improvement over bare carbon due to mixed-valence nanocrystalline patches here and there on the carbon fibers. Its areal capacitance was approximately 0.65 F/cm^2, better than unloaded prepared CFP's areal capacitance of 0.45 F/cm^2.

In all cases the capacitance was relatively level with galvanic charge-discharge cycling rates from 5-20 mA/cm^2 per second.

6.2. Recommendations for Further Work

6.2.1. Methods to improve the gravimetric capacitance

6.2.1.1. Nanofibers

As frequently demonstrated in the literature, pseudocapacitance is boosted when CNT are incorporated in any way, due to the enormous increase in surface area per cm^3 and improved current-carrying network. The incipient wetness solutions could be applied

to carbon nanofibers of diameter of 100's of nm. The active surface area would be increased and the electrolyte spaces would be smaller and more evenly dispersed. If the same volume of VOx per cm^2 could effectively coat the nanofibers, higher specific capacitance would be attained.

The concentrations used in this study were the same as those used in the capillary tube-in-tube studies [42] (Figure 18), but the carbon 'landscape' was different. As this study represents large fibers and the tube-in-tube study represents very small fibers, carbon nanofibers with diameters in the 100's of nanometers would represent a middle ground. The high concentrations used in this study adhered well and distributed evenly in both carbon-landscape extremes, so it is predicted that this study's high-concentration solutions would also coat well on carbon nanofibers.

6.2.1.2. Thinness and conformality of the VOx coating

Thinner coating on the commercial fibers would improve capacitance, because in pseudocapacitance, anything below the top few nm is considered inactive bulk. The coating of VOx could possibly be improved three ways: using smaller fiber to provide greater surface area over which the capillary action could spread the coating; improving the attraction between carbon and the coating; and optimizing the concentration and pH of the solution.

It is possible that using nanofibers might improve the capillary action, around which the incipient wetness impregnation method is based. First, the broad zones of carbon resin would be gone; second, the fibers might be functionalized differently than this study's CFP for better vanadium-attracting surface; third, the space would be more

filled with carbon surfaces over which to spread; and fourth, the curvature of small-diameter fibers might enhance capillary action.

Perhaps the thermal activation of CFP could be optimized for the solution conditions, if the mechanical stability of the CFP could be maintained. However, the attraction between carbon and solution might be more easily improved by changing the solution. Research has shown that bare carbon annealed under oxygen has an acidic surface [45], which means it would attract negative ions. [65] This would predict that solutions with a basic or neutral pH might adhere better than those of acidic pH. This relates to the concept of "point of zero charge" (pzc). Further efforts could be directed to optimize the pH of incipient wetness impregnation solutions for greater attraction to the carbon, resulting in thinner, more conformal coating.

By varying concentration and pH of the incipient wetness solution, over the course of this study, coating varied widely from relatively flat to greatly clumped. This work represents the best-coating combinations found, but work could be continued further to optimize the solution.

6.2.2. Electrochemical testing methods

6.2.2.1. Three-electrode cell

Use of a three-electrode cell would enable identification of the precise voltage(s) at which pseudocapacitive action occurs; this would help define the mechanism.

6.2.2.2. Expand Voltage Range

It is quite likely that some redox behavior was missed by the choice of electrolyte and working voltage. The 4+/5+ redox couple occurs at ~1V, the 3+/4+ couple at ~0.3V

and the 2+/3+ couple at ~-0.25V.[66] Greater pseudocapacitor activity would be utilized by extending the range to exceed 1V.

6.2.2.3. Change the electrolyte

A change of electrolyte to non-aqueous would be necessary to extend into and above the 1V range of testing.

Furthermore, many vanadium species dissolve readily in water, or go in and out of solution with small changes in the local environment (pH, electric field, concentration). Using an appropriate non-aqueous electrolyte would provide a more stable environment for electrochemical testing.

6.2.2.4. Long-term testing

Long-term cycling would be important to study the durability of the oxides and nanostructures.

6.2.3. Fabrication Minor Adjustments

These adjustments could be attempted for further optimization exploration.

Anneal for longer times, but keep the temperature low.

Use a Reflux tube while preparing larger amounts of solution.

Attempt more pH-basic solutions.

Try more variations on the solutions of vanadium concentration >1M.

REFERENCES

1. Zhang, Y., et al., *Progress of electrochemical capacitor electrode materials: A review.* International Journal of Hydrogen Energy, 2009. **34**: p. 4889-4899.

2. Scherson, D.A. and A. Palencsár, *Batteries and Electrochemical Capacitors.* The Electrochemical Society Interface, 2006. **15**(1): p. 17-22.

3. Engstrom, A.M. and F.M. Doyle, *Exploring the cycle behavior of electrodeposited vanadium oxide electrochemical capacitor electrodes in various aqueous environments.* Journal of Power Sources, 2013. **228**: p. 120-131.

4. Qu, Q.T., et al., *Electrochemical behavior of V2O5·0.6H2O nanoribbons in neutral aqueous electrolyte solution.* Electrochimica Acta, 2012. **96**: p. 8-12.

5. Conway, B.E., V. Birss, and J. Wojtowicz, *The role and utilization of pseudocapacitance for energy storage supercapacitors.* Journal of Power Sources, 1997. **66**: p. 1-14.

6. Gujar, T.P., et al., *Spray deposited amorphous RuO2 for an effective use in electrochemical supercapacitor.* Electrochemistry Communications, 2007. **9**: p. 504-510.

7. Greenwood, N.N., *Chemistry of the Elements*, W. Earnshaw, Editor. 1997, Elsevier.

8. Kelsall, G.H., I. Thompson, and P.A. Francis, *Redox chemistry of H2S oxidation by the British Gas Stretford process Part IV: V-S-H2O thermodynamics and aqueous vanadium (v) reduction in alkaline solutions.* Journal of Applied Electrochemistry, 1993. **23**: p. 417-426.

9. Livage, J., *Vanadium Pentoxide Gels.* Chemistry of Materials, 1991. **3**(4): p. 578-593.

10. Augustyn, V. and B. Dunn, *Vanadium oxide aerogels: Nanostructured materials for enhanced energy storage.* Comptes Rendus Chimie, 2010. **13**: p. 130-141.

11. Khan, M.I., et al., *Synthesis and Characterization of Binuclear Oxo-Vanadium Complexes of Carbon Oxoanion Ligands. Crystal Structures of the Binuclear Vanadium(1V) Complex (NH4)[V202(OH)(C404)2(H20)3-H20, of the Mixed-Valence Vanadium(V)/Vanadium(IV)-Squarate Species [(n-C4H9)4N] [V2O3(C4O4)2(H2O)3]-3H2O and [(C4H9)4N]4[V406(C404)5(H20)4-6H20, and of the Binuclear Vanadium(IV) -Oxalate Species [V202Cl2(C204)(CH3OH)4]-2Ph4Cl.* Inorganic Chemistry, 1994. **33**(26): p. 6340-6350.

12. Weckhuysen, B.M. and D.E. Keller, *Chemistry, spectroscopy and the role of supported vanadium oxides in heterogeneous catalysis.* Catalysis Today, 2003. **78**: p. 25-46.

13. Lutta, S.T., et al. *Vanadium Oxide Nanofibers and Vanadium Oxide Polyaniline Nanocomposite: Preparation, Characterization and Electrochemical Behavior*. in *Materials Research Society Symposium*. 2004.

14. P. Adelbert, N.B., N. Gharbi, J. Livage, *Layered structure of vanadium pentoxide gels.* Mat. Res. Bull., 1981. **16**: p. 669-676.

15. Legendre, J.-J.L., Jacques, *Vanadium Pentoxide Gels: I. Structural Study by Electron Diffraction.* Journal of Colloid and Interface Science, 1983. **94**(1): p. 75-83.

16. Legendre, J.-J.A., I.Pierre; Baffier, Noel; Livage, Jacques, *Vanadium Pentoxide Gels: II. Structural Study by X-Ray Diffraction.* Journal of Colloid and Interface Science, 1983. **94**(1): p. 84-89.

17. K. West, B.Z.-C., T. Jacobsen, S. Skaarup, *Vanadium oxide xerogels as electrodes for lithium batteries.* Electrochimica Acta, 1993. **39**(9): p. 1215-1220.

18. Stojkovic, I., et al., *Electrochemical Behaviour of V2O5 Xerogel and V2O5 Xerogel/C Composite in an Aqueous LiNO3 and Mg(NO3)2 Solutions.* Acta Physica Polonica A, 2009. **117**(5): p. 837-840.

19. Dunn, D.R.B., *Electrically conductive oxide aerogels: new materials in electrochemistry.* Journal of Materials Chemistry, 2001. **11**: p. 963-980.

20. Mohan, V.M., K. Murakami, and W. Chen, *The influence of PEO on the synthesis and electrochemical properties of VO2 and V3O7·nH2O nanobelts as a cathode for lithium battery.* Ionics, 2012. **18**: p. 607-614.

21. Li, G., et al., *Environmentally friendly chemical route to vanadium oxide single-crystalline nanobelts as a cathode material for Lithium-ion batteries.* Journal of Physical Chemistry B, 2006. **110**: p. 9383-9386.

22. Pan, A., et al., *Facile synthesized nanorod structured vanadium pentoxide for high-rate lithium batteries.* Journal of Materials Chemistry, 2010. **20**: p. 9193-9199.

23. Menezes, W.G., et al., *V2O5 nanoparticles obtained from a synthetic bariandite-like vanadium oxide: Synthesis, characterization and electrochemical behavior in an ionic liquid.* Journal of Colloid and Interface Science, 2009. **337**: p. 586-593.

24. Oka, Y., T. Yao, and N. Yamamoto, *Structure determination of H2V3O8 by powder x-ray diffraction.* Journal of Solid State Chemistry, 1990. **89**(2): p. 372-377.

25. Legagneur, V., et al., *New layered vanadium oxides MyH1-yV3O8-nH2O (M=Li, Na, K) obtained by oxidation of the precursor H2V3O8.* Journal of Materials Chemistry, 2000. **10**: p. 2805-2810.

26. Zhang, Y., et al., *Controlled synthesis and electrochemical properties of vanadium oxides with different nanostructures.* Bulletin of Materials Science, 2012. **35**(3): p. 369-376.

27. Ren, M.M., et al., *Core-Shell Li3V2(PO4)3@C Composites as Cathode Materials for Lithium-Ion Batteries.* Journal of Physical Chemistry C, 2008. **112**(14): p. 5689-5693.

28. Lee, H. and J. Goodenough, *Ideal Supercapacitor Behavior of Amorphous V2O5-nH2O in Potassium Chloride (KCl) Aqueous Solution.* Journal of Solid State Chemistry, 1999. **148**: p. 81-84.

29. Wang, G., et al., *LiCl/PVA Gel Electrolyte Stablilzes Vanadium Oxide Nanowire Electrodes for Pseudocapacitors.* Acs Nano, 2012. **6**(11): p. 10296-10302.

30. Chen, Z., et al., *Design and Synthesis of Hierarchical Nanowire Composites for Electrochemical Energy Storage.* Advanced Functional Materials, 2009. **19**: p. 3420-3426.

31. Li, H.X., et al., *High-performance Cu-doped vanadium oxide (CuxV2O5) prepared by rapid precipitation method for rechargeable batteries.* Materials Letters, 2007. **61**: p. 101-104.

32. Reddy, R., *Porous structured vanadium oxide electrode material for electrochemical capacitors.* Journal of Power Sources, 2006. **156**: p. 700-704.

33. Kim, I.-H., et al., *Synthesis and Electrochemical Characterization of Vanadium Oxide on Carbon Nanotube Film Substrate for Pseudocapacitor Applications.* Journal of The Electrochemical Society, 2006. **153**(6): p. A989-A996.

34. Huang, C.-M., et al., *Pseudocapacitive Characteristics of Vanadium Oxide Deposits with a Three-Dimensional Porous Structure.* Journal of The Electrochemical Society, 2009. **156**(8): p. A667-A671.

35. Lao, Z.J., et al., *Synthesis of vanadium pentoxide powders with enhanced surface-area for electrochemical capacitors.* Journal of Power Sources, 2006. **162**: p. 1451-1454.

36. Dong, W., J.S. Sakamoto, and B. Dunn, *Electrochemical properties of vanadium oxide aerogels.* Science and Technology of Advanced Materials, 2003. **4**: p. 3-11.

37. Reddy, C.V.S., et al., *Cathodic performance of (V2O5 + PEG) nanobelts for Li ion rechargeable battery.* Journal of Power Sources, 2007. **166**: p. 244-249.

38. Ni, J., et al., *Electrochemical performance of B and M phases VO2 nanoflowers.* Cryst. Res. Tech., 2011. **46**(5): p. 507-510.

39. Steiner, P., *Activation of Coal*. 1981, Foster Wheeler Energy Corporation: United States of America. p. 4.

40. Fischer, A.E., et al., *Incorporation of Homogeneous, Nanoscale MnO2 within Ultraporous Carbon Structures via Self-Limiting Electroless Deposition: Implications for Electrochemical Capacitors.* Nano Letters, 2007. **7**(2): p. 281-286.

41. Deo, G. and I.E. Wachs, *Predicting Molecular Structures of Surface Metal Oxide Species on Oxide Supports under Ambient Conditions.* Journal of Physical Chemistry, 1991. **95**(15): p. 5889-5895.

42. Hu, Y.-S., et al., *Synthesis and Electrode Performance of Nanostructured V2O5 by Using a Carbon Tube-in-Tube as a Nanoreactor and an Efficient Mixed-Conducting Network.* Angewandte Chemie International Edition, 2009. **48**: p. 210-214.

43. K. Jeyalakshmi, S.V., S. Nagamuthu, G. Muralidharan, *Effect of annealing temperature on the supercapacitor behaviour of b-V2O5 thin films.* Materials Research Bulletin, 2013. **48**: p. 760-766.

44. Merdrignac-Conanec, O., K.E. Badraoui, and P. L'Haridon, *Nitridation under ammonia of high surface area vanadium aerogels.* Journal of Solid State Chemistry, 2005. **178**: p. 218-223.

45. Sun, B. and M. Skyllas-Kazacos, *Modification of graphite electrode materials for vanadium redox flow battery application- I. Thermal treatment.* Electrochimica Acta, 1992. **37**(7): p. 1253-1260.

46. Karakoulia, S.A., K.S. Triantafyllidis, and A.A. Lemonidou, *Preparation and characterization of vanadia catalysts supported on non-porous, microporous and mesoporous silicates for oxidative dehydrogenation of propane (ODP).* Microporous and Mesoporous Materials, 2008. **110**: p. 157-166.

47. Li, G., et al., *Synthesis of Urchin-like VO2 Nanostructures Composed of Radially Aligned Nanobelts and Their Disassembly.* Inorganic Chemistry, 2009. **48**(3): p. 1168-1172.

48. Yang, L., et al., *Hierarchical Network Architectures of Carbon Fiber Paper Supported Cobalt Oxide Nanonet for High-Capacity Pseudocapacitors.* Nano Letters, 2012. **12**: p. 321-325.

49. Tang, Q., Y. Chen, and Y. Yang, *Understanding the nature of vanadium species supported on activated carbon and its catalytic properties in the aerobic*

oxidation of aromatic alcohols. Journal of Molecular Catalysis A: Chemical, 2010. **315**: p. 43-50.

50. Oyama, S.T., et al., *Oxygen chemisorption and laser Raman spectroscopy of unsupported and Silica-supported Vanadium Oxide catalysts.* Journal of Physical Chemistry, 1989. **93**(18): p. 6786-6790.

51. Bond, G.C., et al., *Structure and reactivity of titania-supported oxides. Part 1: Vanadium oxide on titania in the sub- and super-monolayer regions.* Applied Catalysis, 1986. **22**: p. 361-378.

52. Stoller, M.D.R., Rodney S., *Best practice methods for determining an electrode material's performance for ultracapacitors* Energy & Environmental Science, 2010. **3**: p. 1294-1301.

53. Khomenkoa, V., E. Frackowiakb, and F. B´eguina, *Determination of the specific capacitance of conducting polymer/nanotubes composite electrodes using different cell configurations.* Electrochimica Acta, 2005. **50**: p. 2499-2506.

54. Chen, L.-M., et al., *Investigations on capacitive properties of the AC/V2O5 hybrid supercapacitor in various aqueous electrolytes.* Journal of Alloys and Compounds, 2009. **467**: p. 465-471.

55. Livage, J., *Hydrothermal synthesis of nanostructured vanadium oxides.* Materials, 2010. **3**: p. 4175-4195.

56. Lampe-Onnerud, C. and J. Thomas, *Mechanisms for the Thermal Decomposition of NH4VO3 into V6O13, V3O7 and V2O5.* Journal of Materials Chemistry, 1995. **5**(7): p. 1075-1080.

57. Chen, L., et al., *Synthesis of Thermochromic W-Doped VO2 (M/R) Nanopowders by a Simple Solution-Based Process.* Journal of Nanomaterials, 2012. **2012**(Article ID 491051): p. 8 Pages.

58. Su, J., et al., *A carbon-coated Li3V2(PO4)3 cathode material with an enhanced high-rate capability and long lifespan for lithium-ion batteries.* Journal of Materials Chemstry A, 2013. **1**: p. 2508-2514.

59. Hurley, B.L., S. Qiu, and R.G. Buchheit, *Raman Spectroscopy Characterization of Aqueous Vanadate Species Interaction with Aluminum Alloy 2024-T3 Surfaces.* Journal of The Electrochemical Society, 2011. **158**(5): p. C125-C131.

60. Wang, X.J., et al., *XRD and Raman study of vanadium oxide thin films deposited on fused silica substrates by RF magnetron sputtering.* Applied Surface Science, 2001. **177**: p. 8-14.

61. Sacken, U.V. and J.R. Dahn, *TGA/MS studies of the thermal decomposition of NH4VO3.* Journal of Power Sources, 1989. **26**: p. 461-465.

62. Volkov, V.L. and G.S. Zakharova, *V3O7· H2O Oxide Nanostructures: Synthesis and Study.* Russian Journal of Inorganic Chemistry, 2009. **54**(11): p. 1704-1707.

63. Kam, K.C. and A.K. Cheetham, *Thermochromic VO2 nanorods and other vanadium oxides nanostructures.* Materials Research Bulletin, 2006. **41**: p. 1015-1021.

64. Cao, Y.W.K.T.K.L.G., *Nanostructured Vanadium Oxide Electrodes for Enhanced Lithium-Ion Intercalation.* Advanced Functional Materials, 2006. **16**: p. 1133-1144.

65. Spieker, W.A. and J.R. Regalbuto, *A fundamental model of platinum impregnation onto alumina.* Chemical Engineering Science, 2001. **56**: p. 3491-3504.

66. Yang, Z., et al., *Electrochemical Energy Storage for Green Grid.* Chemical Reviews, 2011. **111**: p. 3577-3613.